AD-A117 262 CARNEGIE-MELLON UNIV PITTSBURGH PA DEPT OF CHEMISTRY F/G 7/4
PROPERTY-STRUCTURE-PROCESSING RELATIONS IN POLYMERIC MATERIALS.(U)
JUL 81 L YEN, D MEITZ, H MARKOVITZ, G C BERRY AFOSR-77-3404

UNCLASSIFIED AFOSR-TR-82-0303 NL

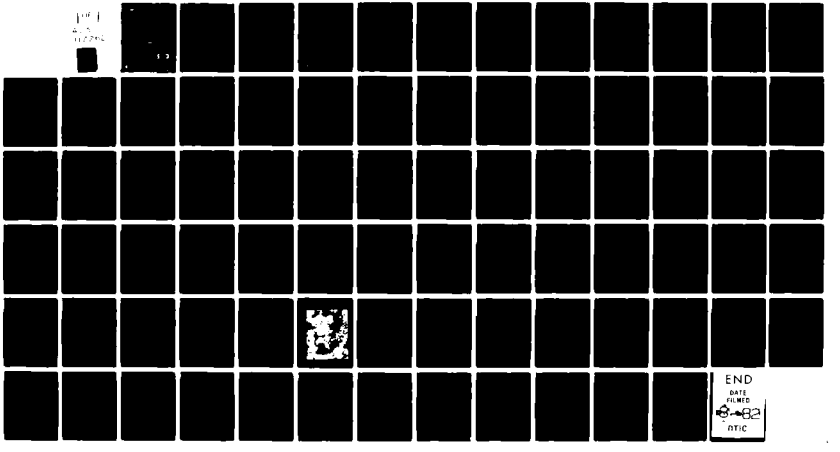

END
DATE FILMED
8-82
DTIC

PROPERTY-STRUCTURE-PROCESSING RELATIONS IN POLYMERIC MATERIALS

Final Report

Grant No. AFOSR-77-3404

31 July 1981

Administrative Report for Management Use
of Air-Force Office of Scientific Research

submitted by

Mellon College of Science
Department of Chemistry
Carnegie-Mellon University
Pittsburgh, PA 15213

UNCLASSIFIED
SECURITY CLASSIFICATION OF THIS PAGE (When Data Entered)

REPORT DOCUMENTATION PAGE	READ INSTRUCTIONS BEFORE COMPLETING FORM
1. REPORT NUMBER: AFOSR-TR- 82-0303	2. GOVT ACCESSION NO. [illegible]
	3. RECIPIENT'S CATALOG NUMBER
4. TITLE (and Subtitle): Property-Structure-Processing Relations in Polymeric Materials	5. TYPE OF REPORT & PERIOD COVERED: Final
	6. PERFORMING ORG. REPORT NUMBER
7. AUTHOR(s): L. Yen, D. Meitz, H. Markovitz, and G. C. Berry	8. CONTRACT OR GRANT NUMBER(s): AFOSR-77-3404
9. PERFORMING ORGANIZATION NAME AND ADDRESS: Carnegie-Mellon University, Department of Chemistry, Pittsburgh, PA 15213	10. PROGRAM ELEMENT, PROJECT, TASK AREA & WORK UNIT NUMBERS: 61102F, 2303/A3
11. CONTROLLING OFFICE NAME AND ADDRESS: Air Force Office of Scientific Research/NC, Bolling AFB, DC 20332	12. REPORT DATE: 31 Jul 1981
	13. NUMBER OF PAGES: 78
14. MONITORING AGENCY NAME & ADDRESS(if different from Controlling Office)	15. SECURITY CLASS. (of this report): Unclassified
	15a. DECLASSIFICATION DOWNGRADING SCHEDULE

16. DISTRIBUTION STATEMENT (of this Report)

Approved for public release; distribution unlimited.

17. DISTRIBUTION STATEMENT (of the abstract entered in Block 20, if different from Report)

18. SUPPLEMENTARY NOTES

19. KEY WORDS (Continue on reverse side if necessary and identify by block number)

Ordered Polymers	Rheology
Rigid Chain Polymers	Suspended Particles
Liquid Crystalline Polymer	Dispensions
Poly(1,4 Phenylene Benzobisoxazole)	Shear Rate
Polymerization Kinetics	Time Dependent Properties

20. ABSTRACT (Continue on reverse side if necessary and identify by block number)

See Other Side

DD FORM 1 JAN 73 1473 EDITION OF 1 NOV 65 IS OBSOLETE

UNCLASSIFIED
SECURITY CLASSIFICATION OF THIS PAGE (When Data Entered)

In recent years, macromolecules with a rodlike chain conformation have been processed from liquid crystalline solutions to prepare fibers and sheets with exceptional stiffness and strength. In this study, the polymerization kinetics of a rodlike chain have been determined. The chain studied, poly(1,4 phenylene benzobisoxazole), PBO, is rigid and rodlike, forms liquid crystalline solutions, and can be fabricated to give high modulus fibers. The investigation showed that the effective reactivity of the chain descreased sharply with increasing chain length. Presumably, this reflects a diffusion-limited polymerization rate for the condensation of rigid rodlike chains--the reactive end group is not free to diffuse without corresponding motion of the entire molecule, in distinction to the situation with flexible-chain polymers. One result of the unusual polymerization kinetics is that the molecular weight distribution is unusually narrow for a step-growth polymer owing to the relative decrease in the production of long chains and the depletion of short chains in the overall population. The second part of this investigation was addressed to the rheological properties of polymeric fluids containing suspended particles. Well-characterized dispersions of spherical particles (crosslinked polystyrene, 0.2 microns in diameter) in a polymer solution (narrow molecular weight distribution polystyrene in dioctyl phthalate) were studied. The viscosity as a function of rate of shear in steady-state shearing flows nx and the time-dependent (visco-elastic) behavior as reflected in R the recoverable compliance obtained by measuring the strain recovered after the stress is removed following steady simple shearing at the shear rate were studied. The behavior observed with these dispersions is qualitatively different from that found with polymer melts and solutions--particularly at low rates of shear. As shear rate decreases, the nx appears to increase indefinitely without indicating actual yield value and R which is a measure of the elastic character of the fluid, approaches a limiting value which can be many orders of magnitude higher than that of the suspending fluid. The dependence of nx and R on the concentration of the suspended particles has been determined. These steady-state measurements were augmented by studies of the creep compliance determined with a shear stress the transient recovery following steady-state deformation under a shear stress and the storage and loss compliances determined at small strain amplitudes. These rheological data thus indicate that the suspensions of beads in a polymeric fluid are solidlike for small imposed strains e.g., imposed strain less than control strain which is approximately .01), and fluidlike for strains in excess of a critical value. Electron microscopy on surface replicas prepared from fractured suspension cooled to the glassy state reveal a substantial order among the beads, which tend to be a hexagonal closepacked array. The rheological data shows that 1) this order is global with irregular aggregates of macroscopic dimensions, even at relatively low bead content, giving the suspension solidlike behavior in shearing deformation (including a deformation for which the strain amplitude is oscillatory in time) provided the strain is smaller than a critical value, and 2) the bead structure may be partially disrupted to permit 'flow' at large strains with the structure retention dependent on the shear rate. It is proposed that the bead structure is stabilized by the loss of entropy suffered by macromolecules in the suspending solution as they come near a bead surface. Organization of the beads is consequently stabilized by osmotic effects that arise owing to reduced polymer concentration in regions between closely spaced beads. Consequently, the suspension develops solidlike properties, even without the intervention of specific attractive forces between the beads or any shape asymmetry that might promote an ordered state. It is believed that the principles elucidated by this study should aid in the understanding of those more complex systems.

TABLE OF CONTENTS

LIST OF FIGURES II

LIST OF TABLES

LIST OF FIGURES III

I ABSTRACT

Suspensions in Polymeric Fluids

The purpose of this part of the investigation was to study the rheological properties of polymeric fluids containing suspended particles. Materials of this type find wide application as sealants, coatings, adhesives, etc.

Under this grant we have chosen to study well-characterized dispersions of spherical particles (crosslinked polystyrene, 0.2 μ in diameter) in a polymer solution (narrow molecular weight distribution polystyrene in dioctyl phthalate or tricresyl phosphate).

To characterize the rheological properties requires a number of different experimental techniques. We have studied (a) η_κ the viscosity as a function of rate of shear in steady-state shearing flows and (b) the time-dependent (viscoelastic) behavior as reflected in R_κ the recoverable compliance obtained by measuring the strain recovered after the stress is removed following steady simple shearing at the shear rate κ.

The behavior observed with these dispersions is qualitatively different from that found with polymer melts and solutions—particularly at low rates of shear. As κ decreases, the η_κ appears to increase indefinitely without indicating an actual yield value and R_κ, which is a measure of the elastic character of the fluid, approaches a limiting value which can be many orders of magnitude higher than that of the suspending fluid. The dependence of η_κ and R_κ on the concentration of the suspended particles has been determined.

These steady-state measurements have been augmented by studies of the creep compliance $J_\sigma(t)$ determined with a shear stress σ, the transient recovery $R_\sigma(t)$ following steady-state deformation under a shear stress σ, and the storage and loss compliances $J'(\omega)$ and $J''(\omega)$, respectively, determined at small strain amplitudes. The results show that $J_\sigma(t)$ is equal to R_0 (the limiting value of $R_\sigma(t)$ for small σ) so long as the imposed strain $\gamma = \sigma J_\sigma(t)$ is smaller than a value γ_c that is small (ca. 0.01) and decreases with increasing bead content. For $\gamma >$

γ_c, $J_\sigma(t)$ deviates from equality with $R_0(t)$ and has a fluid-like limiting behavior with $\partial J_\sigma(t)/\partial t = \eta_\kappa^{-1}$, where η_κ is the parameter defined above. For $\gamma < \gamma_c$, J(t) is found to be equal to the dynamic compliance $|J^*(\omega)|$ for $\omega = t^{-1}$ (here, $|J^*|^2 = (J')^2 + (J'')^2$); this correspondence, while not rigorous, is frequently observed with diverse materials.

These rheological data thus indicate that the suspensions of beads in a polymeric fluid are solidlike for small imposed strains (e.g., for $\gamma < \gamma_c \simeq 0.01$), and fluidlike for strains in excess of a critical value. Electron microscopy on surface replicas prepared from fractured suspensions cooled to the glassy state reveal a substantial order among the beads, which tend to be an hexagonal close-packed array. The rheological data shows that 1) this order is global with irregular aggregates of macroscopic dimensions, even at relatively low bead content, giving the suspensions solidlike behavior in shearing deformation (including a deformation for which the strain amplitude is oscillatory in time) provided the strain is smaller than a critical value, and 2) the bead structure may be partially disrupted to permit 'flow' at large strains with the structure retention dependent on the shear rate.

It is proposed that the bead structure is stabilized by the loss of entropy suffered by macromolecules in the suspending solution as they come near a bead surface. Organization of the beads is consequently stabilized by osmotic effects that arise owing to reduced polymer concentration in regions between closely spaced beads. Consequently, the suspension develops solidlike properties, even without the intervention of specific attraction forces between the beads or any shape asymmetry that might promote an ordered state. It is believed that the principles elucidated by this study should aid in the undertaking of those more complex systems.

Kinetics of Polymerization of Rodlike Macromolecules

In recent years, macromolecules with a rodlike chain conformation have been processed from liquid crystalline solutions to prepare fibers and sheets with exceptional stiffness and strength. In this study, the polymerization kinetics of a rodlike chain have been determined.

The chain studied, poly(1,4 phenylene benzobisoxazole), PBO, is a rigid and rodlike, forms liquid crystalline solutions, and can be fabricated to give high modulus fibers. The investigation showed that the effective reactivity of the chain decreased sharply with increasing chain length. Presumably, this reflects a diffusion-limited polymerization rate for the condensation of rigid rodlike chains—the reactive end group is not free to diffuse without corresponding motion of the entire molecule, in distinction to the situation with flexible-chain polymers. One result of the unusual polymerization kinetics is that the molecular weight distribution is unusually narrow for a step-growth polymer owing to the relative decrease in the production of long chains and the depletion of short chains in the overall population.

II RHEOLOGICAL PROPERTIES OF SUSPENSIONS OF PARTICLES IN POLYMERIC FLUIDS

L. Yen, D. Meitz, H. Markovitz, and G. C. Berry

1 INTRODUCTION

The rheological properties of suspensions of crosslinked polystyrenes spheres (nominally 200 nm diameter) in a fluid comprised of polystyrene (M_w = 411,000) dissolved in either dioctyl phthalate or tricresyl phosphate (0.15 weight fraction dissolved polymer in either solvent) have been studied over a range of concentration of the suspended spheres (0.05, 0.10, 0.15, and 0.20 weight fraction in the polymer fluid).

The objective has been to systematically explore the rheological behavior over a wide range of response time at several temperatures to elucidate the effect of the suspended particles. It has been found that the suspended particles greatly modify the rheological behavior, making the response extremely nonlinear, and sensitive to the strain. It appears that the suspensions studied are essentially solidlike (i.e., the viscosity is either extremely large, or infinite) if the imposed strain is less than some critical value γ_c; for the suspension studied γ_c is about 0.01 – 0.04, depending on the particle concentration. For larger imposed strains, the suspensions incur nonrecoverable deformation, with a viscosity that depends markedly on shear rate even for very slow flows.

The rheological behavior summarized above is attributed to an entropically induced local organization of the spheres in close packed arrays, that develops to form a three dimensional network at the particle concentrations studied. The restriction of chain conformations near the surface of the particles is believed to provide the entropic driving force for the organizations of the particle into arrays that tend to limit the particle surface in contact with the polymer chains.

2 EXPERIMENTAL

A latex containing spherical cross-linked (by copolymerization with divinylbenzene) polystyrene particles with a narrow distribution of sizes, nominally 200 nm in diameter, was supplied by Gerald M. Choi in the laboratory of I. M. Krieger of Case Western University. Ionic surfactants and free electrolytes had been removed by use of an ion-exchange resin. Exchange of organic solvent for the aqueous medium was achieved by dialysis. About 20 ml of the latex was first diluted with 10 ml of methanol. The mixture was then placed in a dialysis bag (Spectrapor 2 membrane) which was then put into a bath containing ca. 2 liters of methanol for three days, the methanol being replaced every 24 hours. The sample was then removed from the dialysis bag and ca. 10 ml of benzene was added. The mixture was then dialysed against benzene according to the same procedure as above. The final product, a suspension of the cross-linked particles in benzene, served as the stock suspension for making the suspensions used in our rheological investigations. The concentration (gm/ml) of the solids in the stock suspension was determined by evaporation of the benzene from a small sample. The cross-linked particles are alternatively called *beads* or *spheres*.

Two suspending media were used: (a) a 15% weight percent solution of linear polystyrene PC-3a in tricresyl phosphate (PS-TCP) and (b) a 15% weight percent solution of the same polystyrene in di-2-ethylhexyl phthalate (PS-DOP). The PC-3a polystyrene was a narrow distribution polymer which according to the manufacturer (Pressure Chemical Co., Pittsburgh, PA) has a molecular weight of 4.1×10^5 with $M_w/M_n \leq 1.06$. Both the TCP and DOP were dried in a vacuum oven at 80°C for 3 days before use. The PC-3a was also dried at 60°C for 2 days.

To prepare suspensions in polymer solutions, dry PS was added to the mixture of the staple suspension with either DOP and TCP. The amount of PS added was such that the final *suspending medium*, which is a PS solution, contains 15% by weight of the linear polymer. The benzene was removed in a rotary evaporator. The final drying was done in a vacuum oven. The following suspensions were prepared: 5%, 10%, 15% and 20% in PS-DOP and in PS-TCP. The concentrations given are in weight %.

Three rheological instruments were used: (a) a rotational cone and plate rheometer incorporating a drag cup torque transducer and a wire suspension whose design and operation has been described (1); (b) a similar rheometer except that air bearings were employed instead of the wire suspension; and (c) a Mechanical Spectrometer (Rheometrics, Inc., Union, NJ, with software and computer components from Science Research Systems of Troy, NY). Creep and recovery data were obtained on the first two instruments at stress levels which extend into the nonlinear region of viscoelastic behavior; the Mechanical Spectrometer was used to perform experiments under sinusoidal stress.

Basic rheological experiments, terminology, symbols, and relations are, for convenience, summarized in Appendix I. More thorough treatments may be found in Ref. 2 and 3. Here we report data on: (a) the viscosity function η_κ as obtained from the rate of shear κ attained in a creep experiment in the steady state, and (b) R_κ the steady-state recoverable compliance as obtained from the final recoverable strain following the steady-state creep experiment, (c) the shear creep compliance $J_\sigma(t)$ from creep experiments, (d) the recovery function $R_\sigma(S,t)$ from recovery following a creep experiment of duration S, and (e) various dynamic mechanical properties obtained by imposing a sinusoidal stress: the storage shear compliance $J'(\omega)$, the loss shear compliance $J''(\omega)$, the absolute value of the complex dynamic shear compliance $|J^*(\omega)|$, and the absolute value of the dynamic viscosity $|\eta^*(\omega)|$.

3 RESULTS

3.1 THE VISCOSITY FUNCTION AND STEADY STATE RECOVERABLE COMPLIANCE

3.1.1 DEPENDENCE ON SHEAR RATE

Figure 1 exhibits data obtained at 50°C on suspensions of the cross-linked polystyrene particles in PS-DOP. Plots of both the viscosity function η_κ (defined by Eqn. A2 of the Appendix) and of the steady state recoverable compliance R_κ (defined by Eqn. A4 of the Appendix) are shown for four concentrations (5,10,15, and 20%) of particles and for the suspending medium itself. The corresponding curves for this system at 30°C have a similar

appearance. To a good approximation, over the range of rates of shear covered, the PS-DOP behaves as a linear viscoelastic material with the viscosity and steady-state compliance independent of the shear rate achieved at steady state during the creep experiment.

As seen in Figure 1, the suspensions have a quite different rheological behavior from the medium in this region of κ where the PS-DOP behaves linearly. As has been observed for many suspensions in polymer fluids (4), the shear stress in steady flow exhibits nonlinearity in the range of κ where the fluid is in the lower Newtonian region. The steady state viscosity function η_κ for the suspensions increases with decreasing κ, attaining values 1000 times greater than the viscosity of the suspending medium. There is no evidence of an approach to a limiting value as κ approaches zero. However, at the upper limit of the experimental range of κ, η_κ appears to approach a plateau level which becomes higher with increasing particle concentration.

As κ approaches zero, the steady-state compliance recoverable function R_κ does appear to approach a limiting value R_0 which depends on the concentration of particles and which is about two orders of magnitude higher than that of the PS-DOP. At the upper end of our range of κ, R_κ decreases to a level close to that of the medium.

Figures 2, 3 and 4 show that η_κ for the suspension in PS-TCP exhibits trends similar to those observed for the PS-DOP suspension. The R_κ for the PS-TSP solution, at the higher rate of shear covered, is in the region of κ where it starts to decrease from its low shear rate value R_0. For these suspensions R_κ remains considerably higher than that for the suspending medium over the entire range of κ.

3.1.2 TEMPERATURE SUPERPOSITION

For polymer melts and solutions, it has been frequently found (5-7) that logarithmic plots of the viscosity function η_κ obtained at various temperatures could be superposed by translations along the axes to obtain a reduced or master graph. This can be expressed by writing

$$\frac{\eta(\kappa,T)}{\eta(0,T)} = \frac{\eta(\kappa a_T,T_0}{\eta(0,T_0)} \tag{1}$$

where the temperature dependence of η_κ has been indicated explicitly by the notation $\eta(\kappa,T)$, T_0 is the arbitrarily selected reference temperature, a_T is the "shift factor" for κ, needed to superpose the data at T to that at T_0, and $\eta(0,T)$ is the zero shear viscosity frequently written as $\eta_0(T)$. Reduced plots of the first normal stress function N_1 for similar materials can also be made according to the relation

$$b_T N_1(\kappa,T) = N_1(\kappa a_T,T_0) \tag{2}$$

where in addition to the shift factor a_T for the κ-axis, a shift factor b_T is required for the N_1 axis. It has been shown that, if such reduced plots are successful, the shift factors can be expressed in terms of the viscoelastic constants:

$$a_T = \eta_0(T)R_0(T)/\eta_0(T_0)R_0(T_0) \tag{3}$$

$$b_T = R_0(T)/R_0(T_0) \tag{4}$$

where $R_0(T)$ is written for $R(0,T)$.

Alternatively, superposition of η_κ is conveniently written as (1.8) (Eqn. A30 of Appendix):

$$\eta(\kappa,T)/\eta_0(T) = Q(\tau_c\kappa) \tag{5}$$

where Q is a function independent of temperature with Q(0) = 1 and where τ_c is a characteristic temperature-dependent time which, for polymer solutions and melts, can be written as

$$\tau_c = \eta_0(T)R_0(T) \tag{6}$$

It is readily seen that the superposition procedure as outlined here cannot be used for our suspensions since, as seen in Figure 1, η_0 is not known and may not exist.

A much less studied superposition is that of R_κ. Data obtained in this laboratory (9) on a number of polymer solutions have indicated the success of such a procedure which can be represented as

$$\frac{R(\kappa,T)}{R(0,T)} = \frac{R(\kappa a_T,T_0)}{R(0,T_0)} \tag{7}$$

or alternatively as (Eqn. A31 of Appendix):

$$R(\kappa,T)/R_0(T) = r(\tau_c\kappa) \tag{8}$$

where r is a temperature-independent function with r(0) = 1 and τ_c is given by Eqn. (6).

While the temperature superposition procedure found to be so useful for polymer melts and solutions could not be applied to our suspensions, a modification did provide a useful representation of the data. When logarithmic plots of R_κ/R_0 versus κ were made, it was

found that the curves for 30° and 50° could be superposed rather well by a horizontal translation along the log κ axis and hence can be described by Eqn. (7) without the identification of a_T given by Eqn. (3). See Figure 5 where the 15% suspension data at 30° have been shifted to superpose on the 50° curve. This procedure can be expressed mathematically as:

$$\frac{R(\kappa,T,\phi)}{R(0,T,\phi)} = \frac{R(\kappa a_T,T_0,\phi)}{R(0,T_0,\phi)} \tag{9}$$

where, for convenience later, we now explicitly indicate the dependence of R_κ on the concentration of particles ϕ as well as on the temperature T by writing $R(\kappa,T,\phi)$. It was found that the same value of log a_T (0.60) was also successful in temperature superposition of the 10% and 20% data.

For the 5% suspension at 50°, data could not be obtained at rates of shear low enough for R_0 to be estimated. If we assume that temperature superposition of R_κ is also valid for the 5% suspension with the same value of a_T which was used for the more concentrated suspensions, then the value of R_0 at 50° can be estimated by shifting the R_κ curve for 50°C vertically until it superposes on the R_κ/R_0 curve for 30°C. Valus of R_0 are listed in Table I.

In the absence of information about η_0 for these suspensions, superposition of the type indicated by Eqn. (1) could not be employed for the viscosity function. However, it was found that the ratio of the viscosity of the suspension to that of the suspending medium could be superposed, *i.e.*:

$$\frac{\eta(\kappa,T,\phi)}{\eta(\kappa,T,0)} = \frac{\eta(\kappa a_T,T_0,\phi)}{\eta(\kappa a_T,T_0,0)} \tag{10}$$

as can be seen for the 15% suspension in Figure 5. For the η_κ data on the 5%, 15%, and

20%, the same a_T, $10^{0.60}$, which was successful for the R_κ data was valid. [For the η_κ curves of the 10% solution, for some unknown reason, a_T was found to be $10^{0.05}$].

Since the η_κ for the solution in this range of κ is in its lower Newtonian region, *i.e.* $\eta(\kappa,T,0) = \eta(0,T,0)$, the zero shear viscosity of the solution could have been written in the denominators of Eqn. (10).

3.1.3 DEPENDENCE ON PARTICLE CONCENTRATION

In the case of polymer solutions a superposition procedure, similar to that used for temperature, has been found applicable for the concentration dependence of linear viscoelastic properties (10) and nonlinear steady state properties, the viscosity and normal stress functions (5,6,11). However, concentration superposition is much less successful than temperature superposition.

Figure 6 indicates that considerable success was achieved in superposing the curves of η_κ and R_κ for various concentrations of particles. The R_κ data seem to follow the relation:

$$\frac{R(\kappa,T,\phi)}{R(0,T,\phi)} = \frac{R(\kappa a_\phi,T,\phi_0)}{R(0,T,\phi_0)} \tag{11}$$

where a_ϕ is the concentration shift factor required to superpose the data for concentration ϕ on that for the reference concentration ϕ_0 here taken to be 20%. Figure 6a indicates the validity for the 50° data; a similar result is obtained for the 30° data with nearly the same value of a_ϕ as seen in Table I and Figure 7. This semilogarthmic plot indicates that the concentration shift factor can be at least roughly approximated by an exponential dependence on ϕ for the 4 concentrations studied:

$$\log a_\phi = 0.80 - 4.0\ \phi$$

For the concentration dependence of η_κ, the analog of neither Eqn. (1) nor Eqn. (10) can be used. It was decided to choose $\eta_p(T,\phi)$ as a reference viscosity level. Here $\eta_p(T,\phi)$ is the value of the viscosity at the point of inflection in the logarithmic plots of η_κ versus κ. Since the point of inflection occurs near the upper limit of our shear rate range, there is some uncertainty as to its precise location. However, since the curves have such a low slope here, there is not much error in the value of log η_p. Reduced plots represented by the relation

$$\frac{\eta(\kappa,T,\phi)}{\eta_p(T,\phi)} = \frac{\eta(\kappa a_\phi,T,\phi_o)}{\eta_p(T,\phi_o)} \tag{12}$$

were attempted where we employed the same a_ϕ as that determined for the superposition of R_κ. Figure 6b shows the results. While the curves for the 10, 15, and 20% suspensions could be superposed rather well, the 5% curve has a different shape and could not be. Values of η_p are listed in Table I. The semilogarithmic plot of η_p versus ϕ shown in Figure 8 indicates that a good straight line could be drawn through the 50° points and a parallel line through the 30° points:

$$\text{At } 30^\circ: \quad \log \eta_p = 2.78 + 4.9\,\phi$$
$$\text{At } 50^\circ: \quad \log \eta_p = 2.16 + 4.9\,\phi$$

Various attempts were made to modify the expression for the reduced viscosity to permit superposition of the 5% curve. Rather good success was achieved by plotting $\log\{[\eta(\kappa,T,\phi)/A(T)]-1\}$ versus $\log \kappa\phi$ where A(T) was found by trial and error A(30°) = 800 poise and A(50°) = 160 poise) and where $A(30^\circ)/A(50^\circ) = \eta(0.30^\circ,0)/\eta(0.50^\circ,0)$. However, since this introduces another arbitrary constant and the extent of our data are not sufficient to test this proposal adequately, we do not present the resulting curves here.

3.2 DYNAMIC COMPLIANCE

3.2.1 BEHAVIOR AT LOW STRAIN AMPLITUDE

Studies of the creep, recovery, and dynamic behavior were used to elucidate the anomalous behavior described above. The dynamic compliance $|J^*(\omega)|$, given in Fig. 9 for each of the suspensions in PS-TCP, were acquired at small enough strain amplitude that $|J^*(\omega)|$ appeared to be independent of the strain amplitude. For the 5% suspension and for the PS-TCP, a short range of ω was observed for which $|J^*(\omega)| \propto \omega^{-1}$; this behavior was not observed with the other fluids studied, for which $\partial \ln |J^*(\omega)| / \partial \ln \omega > -1$ over the available frequency range. This behavior will be discussed further after the creep results have been described. Except for the 20% suspension (see below), data obtained at various temperatures could be superposed, and it is the resultant superposed curves which are given in Figure 9.

The compliances $J'(a_T\omega)$ and $J''(a_T\omega)$ for the PS-TCP suspensions are shown in Figs. 10-11. The J" data at the lowest ω reached for the 15 and 20% suspensions have not attained the limiting proportionality with $(a_T\omega)^{-1}$ as expected for a viscoelastic fluid, so that η_0 must be either very large or infinite (e.g., see Eqn. A21). It is evident that the available range in $a_T\omega$ is not sufficient to fully characterize the viscoelastic properties of the suspensions studied in that the effects of very long retardation times are not seen due to the truncation of the data at low $a_T\omega$; the creep and recovery data discussed below compensate for this lack. Values of a_T are discussed below.

Not all of the dynamic data could be treated by a time-temperature equivalence using empirically determined shift factors a_T and b_T (rather than calculating them from Eqns. A25-26)). For example, $J'(\omega)$ and $J''(\omega)$ for the 20% suspension at several temperatures shown in Figs. 12-13 could not be so treated; similar behavior is seen in Fig. 14 for $|J^*(\omega)|$. At the present, the source of this behavior is unknown, see below. In Fig. 12-13, a_T has been selected to provide superposition in the low frequency range; the data in Figs. 10 and 11 were limited to the latter range for the 20% suspension. No difficulty was found for the less concentrated solutions.

3.2.2 BEHAVIOR AT LARGE STRAIN AMPLITUDE

In sinusoidal deformations of suspensions of concentration greater than 5%, the measured $|J^*(\omega)|$ is a function of the strain amplitude γ_0 when γ_0 is of the order of γ_c or larger and thus the behavior no longer follows linear viscoelasticity. It is found that $|J^*(\omega)|$ increases as γ_0 increases. The direction of this change is similar to the increase of $J_\sigma(t)$ with increasing σ when the strain becomes larger than γ_c. However, an exact correlation of these two functions has yet to be found.

3.2.3 TEMPERATURE DEPENDENCE

The temperature dependence of a_T as determined from the oscillatory measurements on the PS-TCP suspensions can be empirically represented by an equation of the Arrhenius type:

$$a_T = e^{(\Delta H_a/R)(1/T - 1/T_c)}$$

where ΔH_a is an apparent energy of activation for flow. The ratio of a_T^w, the shift factor for the rheological functions of the suspensions, to a_T^s, the shift factors for the solution is shown in Fig. 15. It is seen that a_T^w/a_T^s is only a slightly increasing function of temperature when the beads are added to the solution, and is almost independent of the bead concentration. This implies that the temperature dependence of the rheological functions of the suspensions are dominated by the polymer solution into which the beads are placed. The small positive value of $\partial \ln(a_T^w/a_T^s)/\partial T$ shown in Fig. 15 is opposite to what might have been expected on this simple premise since the uptake of solvent by the added beads would increase the concentration of the polymer solution external to the beads. The magnitude of ΔH_a is 4 kcals/mole as would be expected in polymer solutions of the type used here to suspend the beads.

3.3 CREEP AND RECOVERY

Examples of the creep compliance $J_\sigma(t)$ determined over a range of applied shear stress σ are given in Figs. 16-18. Also included are examples of $R_\sigma(S,t)$, the recoverable compliance measured after a creep experiment of duration S with shear stress σ--for S so large that $R_\sigma(S,t)$ had (essentially) reached the asymptotic limit $R_\sigma(\infty,t)$. For the 10 and 15% suspensions, $J_\sigma(t)$ is approximately equal to $R_0(\infty,t)$ for $\gamma(t)$ less than a value γ_c, that is more or less independent of σ. For $\gamma(t) > \gamma_c$, $J_\sigma(t)$ changes, over a relatively short range of strain, to behavior such that $J_\sigma(t) \sim t/\eta_\kappa + R_\sigma(\infty,t)$. Moreover, if the stress is removed at time S such that $\gamma(S) < \gamma_c$, then $R_\sigma(S,t)$ can be estimated by use of the linear Boltzmann relation in the form (cf. Eqn. A14 of the Appendix):

$$R_\sigma(S,t) = J_\sigma(S) + J_\sigma(t) - J_\sigma(t+S) \tag{14}$$

with

$$J_\sigma(t) = R_\sigma(\infty,t)+t/\eta_0 \tag{15}$$

For the materials studied here, in such cases η_0 is extremely large (e.g., $\eta_0 >$ ca 10^9 poise), so that $J_\sigma(t) \sim R_0(\infty,t)$ for $\gamma(t) < \gamma_c$. As shown in Figs. 14-17, for these materials, $|J^*(\omega=t^{-1})|$ is within experimental error equal to $J_\sigma(t)$ for the entire region of overlap. These results show that the material is essentially solidlike, both in creep until $\gamma(t) > \gamma_c$, and in oscillatory strain at low strain amplitude; the value of γ_c is about 0.02 and 0.01 for the 10 and 15% materials, respectively. In this context, the short range of ω over which $\partial \ln |J^*(\omega)| / \partial \ln \omega \simeq -1$ is seen as a manifestation of $R_0(t)$ rather than as a sign of the flow regime (e.g., Eqns. (A20-21)). Presumably, at still smaller ω, $|J^*(\omega)|$ would tend to reach an asymptotic limit, equal to R_0; the creep and recovery data show that the ω required to reach such a limit is well below the available range for the suspensions studied.

A similar pattern appears to obtain even with the 5% suspension, but the studies are much more difficult owing to the low stress levels that must be employed to effectively study the long retardation times inherent in the suspensions studied. In large measure, this reflects the magnitude of R_0 and the nature of $R_0(t)$. For example, as shown in Fig. 19, for the suspensions studied, $R_0 \propto w^{-2}$, where w is the weight fraction of the suspended particles. The creep and recovery data (Fig. 16) for the 5% suspension are less conclusive concerning solidlike behavior at low strain than the data for the more concentrated suspensions, but it does appear that $J_\sigma(t)$ and $R_\sigma(\infty,t)$ are very close (e.g., t/η_0 is small in comparison with $R_\sigma(\infty,t)$) for small strains. For larger strains (e.g., $\gamma(t)$ > ca 0.001), the $J_\sigma(t)$ at different σ do not superpose. This may be due to experimental error (e.g., unidentified extraneous instrumental torques contributing to the sample deformation) or to an nonreproducible, metastable structure in the sample. We suspect the latter is the case, with some support from the steady-state flow behavior shown in Fig. 2.

3.4 MAGNITUDE OF THE COMPLEX VISCOSITY

A widely used empirical rheological rule is the Cox-Merz relation which states that the steady-state viscosity η_κ is equal to the $|\eta^*(\omega)|$ of linear viscoelasticity at a value of the angular frequency ω equal to the shear rate κ (12).

At small strain amplitudes, where linear viscoelasticity holds, it is found that $|\eta^*(\omega=\kappa)|$ is greater than η_κ for the 20% and 15% suspensions in PS-TCP. A possible rationale for this deviation is the fact that η_κ is measured at $\gamma >> \gamma_c$ while $|\eta^*(\omega)|$ is measured at strain amplitudes less than γ_c. Fig. 4 illustrates such behavior for the 15% suspension.

For the 5% suspension, $|\eta^*(\omega)|$ was found to be independent of the amplitude of strain as was the case for the solution without beads. As seen in Fig. 2, the Cox-Merz relation was found to be valid for this suspension.

4 DISCUSSION

The data presented above demonstrate that for $\gamma(t) > \gamma_c$, these materials become fluidlike, with an apparent steady-state viscosity $\eta_\kappa = \sigma/\kappa$ that displays the peculiar features shown in Figs. 2-4. The observation that at low σ, $R_\sigma(\infty,t)$ is about equivalent to $J_\sigma(t)$ for $\gamma(t) < \gamma_c$ is remarkable. Presumably, the abrupt change in rheological behavior that occurs for $\gamma(t) > \gamma_c$ is due to a breakdown of a three-dimensional organization among the suspended spheres. Nonetheless, after cessation of flow, the recovery is equivalent to what would be expected if the organization had remained intact. Similar behavior has been reported for weak, reversible polymeric gels (13). The behavior found with the 10 and 15% suspensions suggests that the three-dimensional structure inherent in the quiescent material is maintained only if the total strain is very small. For larger strains, the structure apparently is degraded into domains, with internal strain similar to that in the organized structure prior to its degradation. The domain size may decrease as the shear rate increases (e.g., η_κ decreases with increasing κ), but we have no direct data to assess this possibility.

Figure 20 is an electron micrographwhich shows that the suspended particles are organized locally into domains with the spheres in a hexagonal close packed array. The rheological data show that these regions of local order have a large enough spatial extent to form a tenuous, macroscopic three dimensional network, perhaps for weight fraction of spheres as low as 5%, but certainly for 10% weight fraction. The original domains may be reversibly deformed, but the network is readily ruptured if the strain exceeds a small limit (which depends on the particle concentration). The network rupture does not lead to a random distribution of sphere positions, but rather locally ordered domains remain in a deformed state. These domains relax and reunite to form larger units if the stress is removed.

The driving force for the local order is speculated to be entropic in nature(14-16). Polymer chains close to a bead surface have fewer conformations available to them than those far from such a surface. Local collapse of the spheres into a close packed array will alleviate this situation. Theoretical studies of the configurational partition function for a system of two spheres separated by a random-flight chain support this model (14-16).

The temperature dependence of the low strain dynamic responses as exhibited in Fig. 15, is an indication that the flow mechanism of the polystyrene solution is not significantly altered by the presence of the suggested structure. The dramatically larger stresses needed for the suspensions to reach steady state flow at $\gamma >> \gamma_c$ as compared to the polystyrene solution at a given rate of shear can thus be seen not to be the result of any larger scale change in the properties of the polystyrene in solution. We attribute it to the deformation of the three-dimensional structure as described above.

It is not unexpected that the Cox-Merz relation fails for the more concentrated suspensions in view of our picture of the deformation mechanisms. The $|\eta^*(\omega)|$ is measured at low γ where the macroscopic aggregates are only slightly deformed. It would be surprising if there were a simple relation between this $|\eta^*(\omega)|$ and η_κ which is determined at high γ where this structure is broken down.

For several suspensions η_κ, at low rates of shear, gives a linear graph when log η_κ is plotted against log κ; i.e., η_κ has a κ^{-a} behavior at low κ. Since $a \neq 1$, this does not correspond to the classical yield stress response. Since no limiting value of η_κ was found at low κ, neither does this behavior correspond to the behavior of the fluids defined in current continuum mechanical theories (i.e., nonlinear viscoelasticity or Noll's simple fluid with fading memory). It would seem worthwhile to develop an appropriate continuum mechanical theory for this case where η_κ increases indefinitely as κ decreases toward zero.

It should be noted that the rheological behavior attributed to the postulated three dimensional network is observed for particle concentration as low as 5%, and is quite marked for a 20% suspension of the spherical particles. We suggest that the behavior elucidated here has an important role in more complex systems. In particular, with asymmetric particles, the entropically driven organization may result in materials which behave as more rigid solids under small imposed strains, while still permitting flow at larger strains, as with materials used as channel-sealants, coatings, etc.

5 REFERENCES

1. G. C. Berry and C.-P. Wong, *J. Polym. Sci., Polym. Phys. Ed.* **13**, 1761 (1975).

2. J. D. Ferry, *Viscoelastic Properties of Polymers*, 3rd ed. Wiley, New York, 1980.

3. H. Markovitz, in *AIP 50th Anniversary Physics Vade Mecum*, H. L. Anderson, Editor-in-Chief, Chap. 19, American Institute of Physics, New York, 1981.

4. See, for example:
   (a) S. Onogi, T. Matsumoto and Y. Warashina, *Trans. Soc. Rheol.* **17**, 175 (1973).
   (b) T. Matsumoto, C. Hitomi and S. Onogi, *Trans. Soc. Rheol.* **19**, 541 (1975).
   (c) N. Minagawa and J. L. White, *J. Appl. Polym. Sci.* **20**, 501 (1976).
   (d) V. M. Lobe and J. L. White, *Polym. Eng. Sci.* **19**, 617 (1979).

5. F. J. Padden and T. W. DeWitt, *J. Appl. Phys.* **25**, 1086 (1954).

6. H. Markovitz, *Trans. Soc. Rheol.* **1**, 37 (1957).

7. H. Markovitz, *J. Polym. Sci., Polym. Symp.* **50**, 431 (1975).

8. W. W. Graessley, *Adv. Polym. Sci.* **16**, 1 (1974).

9. C.-P. Wong and G. C. Berry, *Polym. Prepr. Am. Chem. Soc. Div. Polym. Chem.* **15**(2), 126 (1974).

10. J. D. Ferry, *J. Am. Chem. Soc.* **72**, 3746 (1980).

11. H. Markovitz and D. R. Brown, *Trans. Soc. Rheol.* **7**, 137 (1963).

12. W. Cox and E. H. Merz, *J. Polym. Sci.* **28**, 619 (1958).

13. C.-P. Wong and G. C. Berry, *Polymer* **20**, 229 (1979).

14. A. Vrij, *Pure Appl. Chem.* **33**, 183 (1958).

15. S. Asakura and F. Oosawa, *J. Polym. Sci.* **33**, 183 (1958).

16. J. F. Joanny, L. Leibler, and P. G. deGennes, *J. Polym. Sci., Polym. Phys. Ed.* **17**, 1073 (1979).

6 APPENDIX

6.1 COMPILATION OF RHEOLOGICAL TERMS, SYMBOLS AND RELATIONS

6.1.1 BASIC EXPERIMENTS AND MATERIAL PROPERTIES

The viscoelastic properties of a material are most readily defined in terms of a few basic experiments:

1) Creep experiment. A shear stress σ is applied at a time t=0 and maintained constant thereafter. The strain $\gamma_\sigma(t)$ for times, $t > 0$, defines the *shear creep compliance* $J_\sigma(t)$:

$$\gamma_\sigma(t) = \sigma J_\sigma(t) \tag{A1}$$

For some materials, called *viscoelastic fluids*, in a creep experiment, a steady state is reached. The rate of shear $d\gamma_\sigma(t)/dt$ approaches a constant value κ as t increases indefinitely. The *viscosity function* η_κ is defined as

$$\eta_\kappa = \sigma/\kappa \tag{A2}$$

2) Recovery experiment. After a creep experiment has proceeded until $t = S$, the shear stress is then removed. From the shear strain at a time θ after the stress is removed, the *recoverable strain* $\gamma^R(S,\theta)$ is defined as

$$\gamma^R(S,\theta) = \gamma_\sigma(S) - \gamma_\sigma(S+\theta) \tag{A3a}$$

and the *recovery function* $R_\sigma(S,\theta)$ is defined:

$$R_\sigma(S,\theta) = \gamma^R(S,\theta)/\sigma \tag{A3b}$$

If the creep of a viscoelastic fluid is permitted to continue until the steady state with the shear rate κ is reached ($S \to \infty$) and then a recovery experiment is allowed to continue indefinitely ($\theta \to \infty$), then $R_\sigma(S,\theta)$ approaches a limit called the *steady state recoverable shear compliance* R_κ:

$$R_\sigma(\infty,\infty) = R_\kappa \tag{A4}$$

3) Stress relaxation experiment. A shear strain γ is applied at $t = 0$ and maintained constant thereafter. The shear stress $\sigma_\gamma(t)$ for times $t > 0$ define the *shear relaxation modulus* $G_\gamma(t)$:

$$\sigma_\gamma(t) = \gamma G_\gamma(t) \tag{A5}$$

4) Ramp experiment. At a time t after a constant shear rate κ is applied, the stress $\sigma(t)$ defines the *shearing viscosity function* $\eta_\kappa(t)$:

$$\eta_{\kappa}(t) = \sigma(t)/\kappa \tag{A6}$$

If the deformation is allowed to proceed until t = S and then stopped, the stress $\sigma(S,\theta)$ at a time θ after the strain stopped defines the *relaxation function* $G_{\kappa}(S,\theta)$:

$$G_{\kappa}(S,\theta) = \sigma(\theta)/\kappa \tag{A7}$$

5) Sinusoidal experiment. If a sinusoidal shear stress $\sigma^*(t) = \sigma_0 e^{i\omega t}$ is imposed, the shear strain in the steady state has a Fourier component of the same frequency which can be represented as $\gamma_1^* = \gamma_0 e^{i(\omega t-\delta)}$. The *complex dynamic shear compliance* $J^*_{\sigma}(\omega)$ is defined by:

$$J^*_{\sigma}(\omega) = \gamma_1^*(t)/\sigma^*(t) = J'_{\sigma}(\omega) - iJ''_{\sigma}(\omega) \tag{A8}$$

where $J'_{\sigma}(\omega)$, the real part of $J^*_{\sigma}(\omega)$, is called the *storage shear compliance* and $J''_{\sigma}(\omega)$, the imaginary part, is called the *loss shear compliance.*

The *complex dynamic viscosity* $\eta^*_{\sigma}(\omega)$ is defined as

$$\eta^*_{\sigma}(\omega) = \sigma^*(t)/\dot{\gamma}_1^*(t) = \eta'_{\sigma}(\omega) - i\eta''_{\sigma}(\omega) \tag{A9}$$

where $\dot{\gamma}_1^*(t)$ is the rate of strain $d\gamma_1^*(t)/dt$, and where $\eta'_{\sigma}(\omega)$ is called the *dynamic viscosity.* It can be readily shown from these definitions that:

$$\eta'_\sigma(\omega) = J''_\sigma(\omega)/\omega\,|J^*_\sigma(\omega)|^2 \tag{A10}$$

$$\eta''_\sigma(\omega) = J'_\sigma(\omega)/\omega\,|J^*_\sigma(\omega)|^2 \tag{A11}$$

where $|J^*_\sigma(\omega)|$, the *absolute value of* $J^*_\sigma(\omega)$, *is*

$$|J^*_\sigma(\omega)|^2 = [J'_\sigma(\omega)]^2 + [J''_\sigma(\omega)^2] \tag{A12}$$

6.1.2 LINEAR VISCOELASTICITY

If the stresses in the above experiments become small, various of the above-defined material function approach limiting values and are interrelated by expressions which can be derived from the theory of linear viscosity.

1) Creep experiment. For sufficiently small stress σ, $J_\sigma(t)$ becomes a stress independent function, $J(t)$ and η_χ becomes a constant η_0, often called the zero shear viscosity. For a linear viscoelastic fluid, one can write $J(t)$

$$J(t) = R_0(t) + t/\eta_0 \tag{A13}$$

where $R_0(t)$ is the limiting value of the recovery function $R_\sigma(\infty,t)$ as σ approaches zero. [The subscript zero is not used in $J(t)$ and other linear viscoelastic properties in order to conform to the standard notation.

2) Recovery experiment. For sufficiently small stress σ, $R_\sigma(S,\theta)$ becomes independent of σ and approaches $R_0(S,\theta)$:

$$R_0(S,\theta) = J(S)-J(S+\theta)+J(\theta) \tag{A14}$$

and the steady state recoverable compliance R_κ approaches a limiting value

$$R_0(\infty,\infty) = R_0(\infty) = R_0 \tag{A15}$$

3) Stress relaxation experiment. For sufficiently small strain γ, the shear relaxation modulus $G_\gamma(t)$ becomes $G(t)$ independent of γ. From the theory of linear viscoelasticity it is shown that $J(t)$ and $G(t)$ are interrelated:

$$\int_0^t J(s)G(t-s)ds = t \tag{A16}$$

and that

$$\eta_0 = \int_0^\infty G(t)dt \tag{A17}$$

$$\tau_c = R_0\eta_0 = \int_0^\infty tG(t)dt \Big/ \int_0^\infty G(t)dt \tag{A18}$$

where τ_c is a useful time constant characterizing viscoelastic behavior.

4) Ramp experiment. When κ is sufficiently small, $\eta_\kappa(t)$ approaches $\eta_0(t)$, a function independent of κ:

$$\eta_0(t) = \int_0^t G(s)ds \tag{A19}$$

5) Sinusoidal experiment. For sufficiently small σ_0, the shear strain in the steady state is $\gamma^*(t) = \gamma_0 e^{i(\omega t-\delta)}$ and the various associated viscoelastic properties become independent of the σ. This is signified by omitting the σ in the subscript, e.g. $J^*_\sigma(\omega)$ goes to $J^*(\omega)$, $J'_\sigma(\omega)$ to $J'(\omega)$, $\eta'_\sigma(\omega)$ to $\eta'(\omega)$, etc.

From the theory of linear viscoelasticity, it is known that

$$J'(\omega) = R_0 - \omega \int_0^\infty [R_0-R_0(t)]\sin \omega t \, dt \tag{A20}$$

$$J''(\omega) = (\omega \eta_0)^{-1}+\omega \int_t^\infty [R_0-R_0(t)]\cos \omega t \, dt \tag{A21}$$

A useful approximation is

$$J(t) \simeq \left| J^*(\omega = t^{-1}) \right| \tag{A22}$$

where we use the notation F(x=z) to mean the value of F(x) for x=z.

6) Retardation spectrum. Another useful method of representing linear viscoelastic behavior is through the use of the *retardation spectrum* $L(\tau_d)$ of *retardation times* τ_d which may be defined by the equation:

$$R_0(t) = J_g + \int_{-\infty}^{\infty} L(\tau_d)[1-\exp\{-t/\tau_d\}]d \ln \tau_d \qquad \text{(A23)}$$

where the *glassy compliance* J_g is $R_0(0)$.

6.1.3 TIME-TEMPERATURE EQUIVALENCE

For many materials (e.g. random coil polymers and their concentrated solutions) the logarithmic plot of J(t) for the temperature T can be superimposed on that for the temperature T_0 (called the reference temperature) by a translation by log a_T along the log t axis and by a much smaller translation, log b_T, along the log J axis. In such a case, using the notation J(t,T) to indicate the function J(t) at the temperature T, we can then write

$$b_T J(t,T) = J(t/a_T, T_0) \qquad \text{(A24)}$$

and plots of $b_T J(t,T)$ for various values of T will fall on one *reduced* graph if plotted against a reduced time t/a_T. The material is said to be *thermorheologically simple* and *time-temperature superposition* is said to be applicable. It can be shown that similar reduced plots can be made for the other viscoelastic function: e.g., $b_T J'(\omega,T)$, $b_T J''(\omega,T)/b_T a_T$ and $\eta'(\omega)/b_T a_T$ versus $a_T\omega$. It can then be shown that, for a viscoelastic fluid, that

$$a_T = \tau_c(T)/\tau_c(T_0) \qquad \text{(A25)}$$

$$b_T = R_0(T_0)/R_0(T) \qquad \text{(A26)}$$

where τ_c, a useful time constant for the material is given by

$$\tau_c = \eta_0 R_0 \tag{A27}$$

Using time–temperature equivalence, Eqn. (A8) can be recast to a form which will give a universal curve for various temperatures:

$$J(t/\tau_c) \simeq R_0[\psi(t/\tau_c) + t/\tau_c] \tag{A28}$$

where

$$\psi(t) = [R_0(t)-J_g]/[R_0-J_g] \tag{A29}$$

The concept of thermorheological simplicity is found to be valid for nonlinear viscoelastic properties as well. Data on η_κ at various temperatures (and to a certain extent at various molecular weights and concentrations c for polymer solutions) fall on a single plot when plotted in the form of η_κ/η_0 versus $\tau_c\kappa$. This is expressed by the equation:

$$\eta_\kappa = \eta_0 Q(\tau_c\kappa) \tag{A30}$$

where $Q(\tau_c\kappa)$ is independent of T (and of c). Typically $Q(\tau_c\kappa)$ exhibits a crossover from $Q(\tau_c\kappa) = 1$ to $Q(\tau_c\kappa) = q(\tau_c\kappa)^{-m}$ behavior at $\tau_c\kappa \simeq 1$. It is also observed that R_κ for various temperatures can be similarly represented by:

$$R_{\kappa} = R_0 P(\tau_c \kappa) \tag{A31}$$

where $P(\tau_c \kappa)$ is independent of temperature.

Table 1: Parameters Used in Superposing R_κ and η_κ Data for Suspension in PS-DOP

ϕ	log R_0		log a_ϕ		log η_p	
	30°	50°	30°	50°	30°	50°
0.00	-4.04	-4.15				
0.05	-1.64	(-1.58)*	0.62	0.50	3.00	2.40
0.1	-1.86	-1.70	0.42	0.38	3.35	2.61
0.15	-2.15	-2.02	0.30	0.20	3.49	2.93
0.20	-2.65	-2.42	0	0	3.70	3.15

* Estimated from superposition procedure [see text].

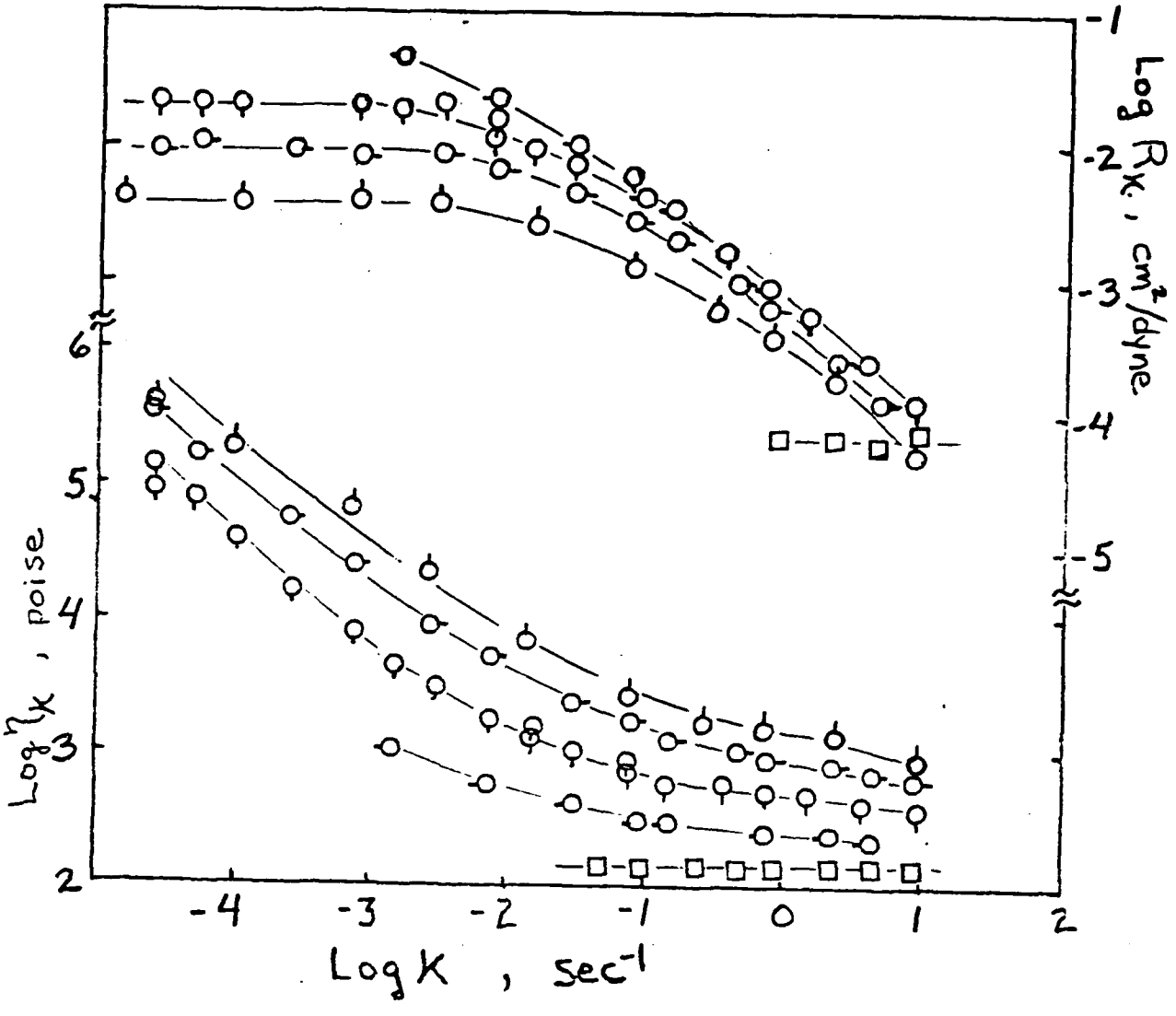

Figure 1:

Plots of the steady-state recoverable compliance and the viscosity function for the suspensions of the cross-linked polystyrene particles in PS-DOP at 50°C. The squares are data for the PS-DOP solution: the circles for the suspensions: pip up 20%; right 15%; down 10%; left 5%.

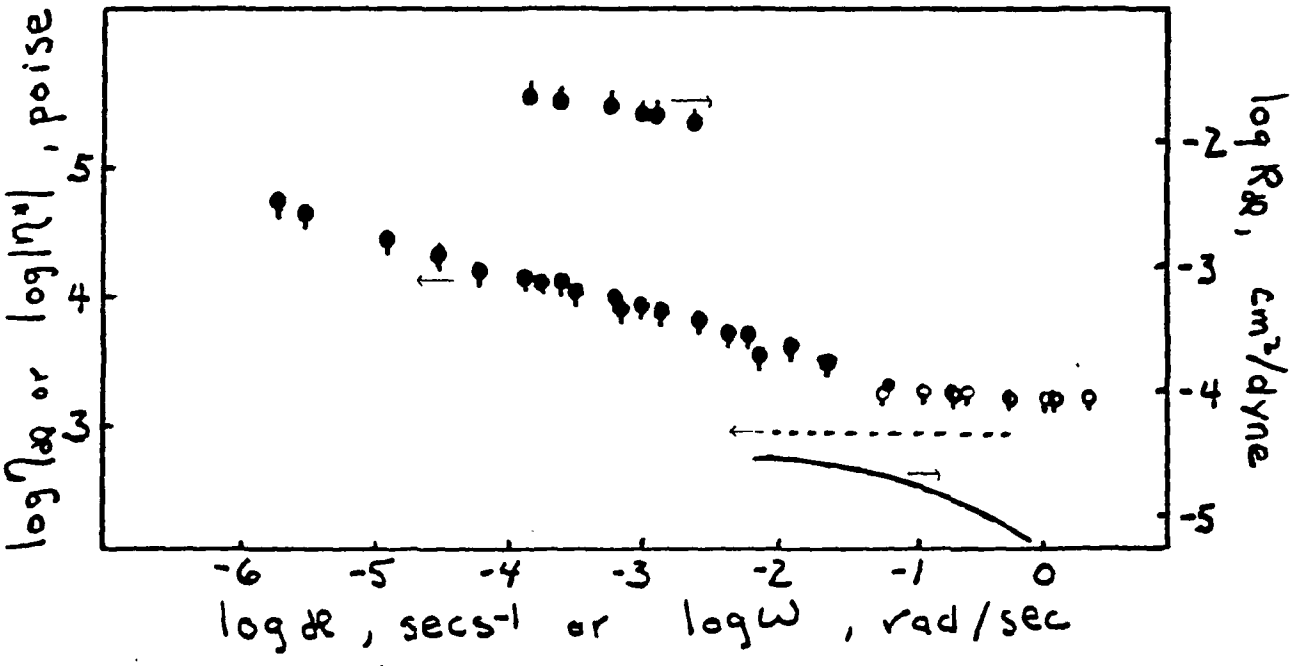

Figure 2:

Data of a 5% suspension of polystyrene beads in PS-TCP. Bilogarithmic plot of the viscosity η_κ, filled and half filled circles (representing data from two instruments) pip down, and the compliance R_κ, filled circles pip up, versus shear rate κ is shown. Also shown is the magnitude of the dynamic viscosity $|\eta^*(\omega)|$, open circles pip down, versus angular frequency ω. The dashed and solid curves represent η_κ and R_κ, respectively, for the solution. All responses are at 33°C.

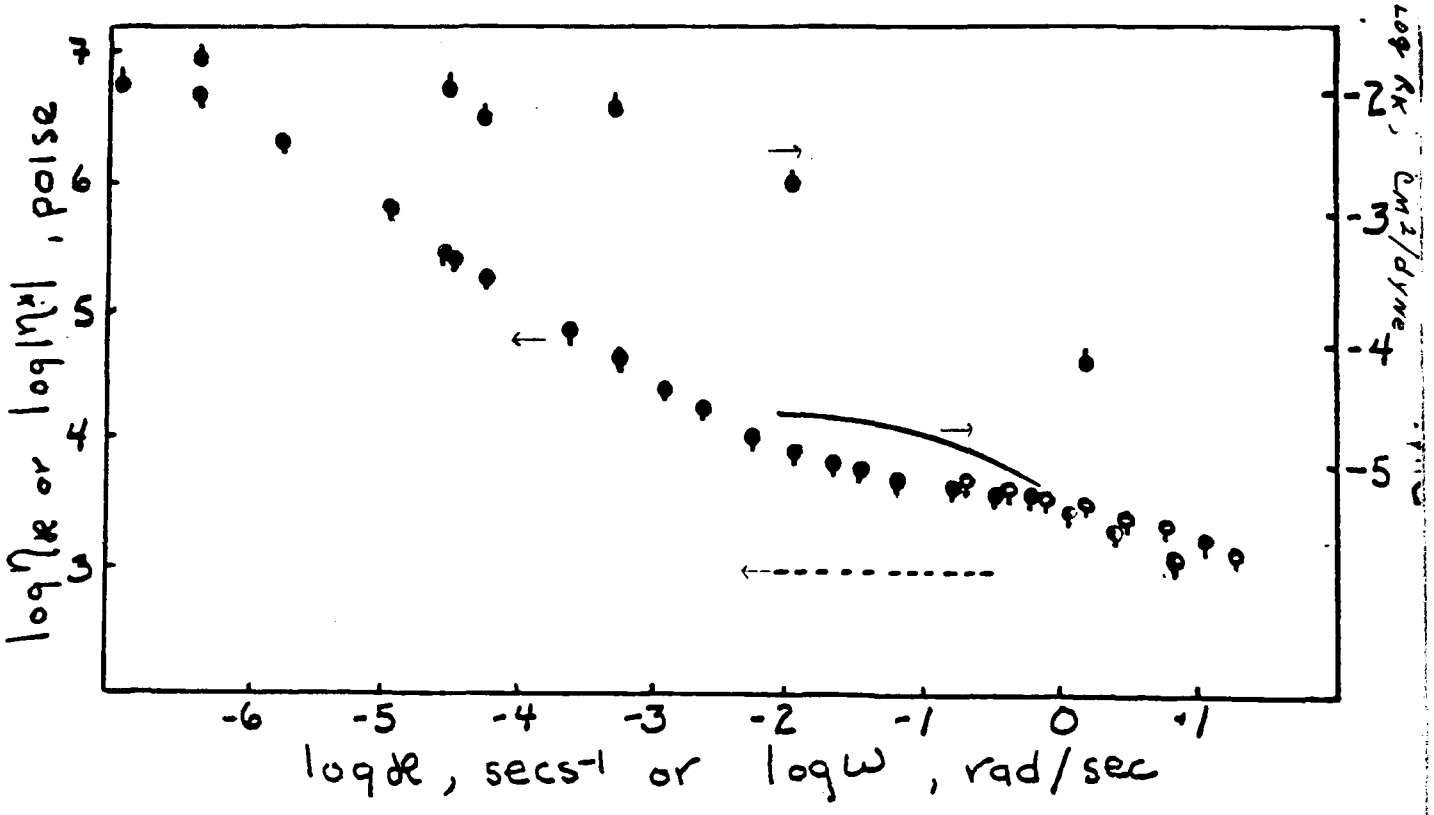

Figure 3:

Data of a 10% suspension of polystyrene beads in PS-TCP. Bilogarithmic plot of the viscosity η_κ, filled and half filled circles (representing data from two instruments) pip down, and the compliance R_κ, filled circles pip up, versus shear rate κ is shown. Also shown is the magnitude of the dynamic viscosity $|\eta^*(\omega)|$, open circles pip down, versus angular frequency ω. The dashed and solid curves represent η_κ and R_κ, respectively, for the solution. All responses are at 33°C.

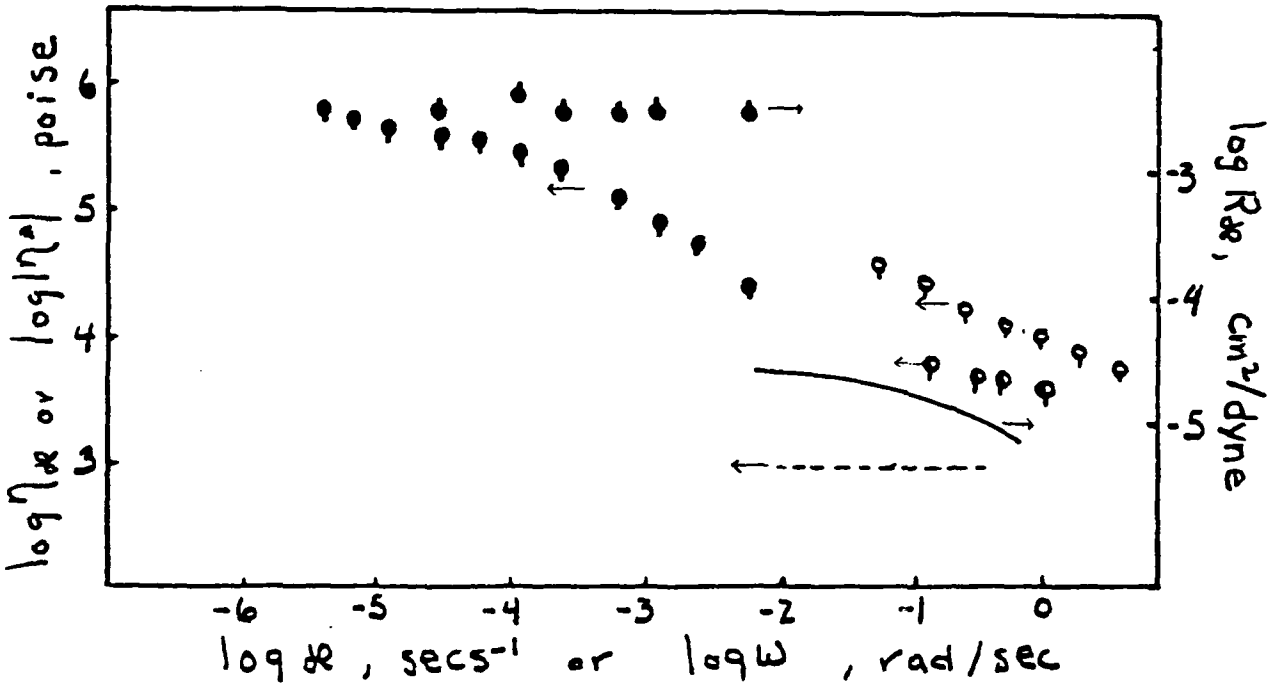

Figure 4:

Data of a 15% suspension of polystyrene beads in PS-TCP. Bilogarithmic plot of the viscosity η_κ, filled and half filled circles (representing data from two instruments) pip down, and the recoverable compliance R_κ, filled circles pip up, versus shear rate κ is shown. Also shown is the magnitude of the dynamic viscosity $|\eta^*(\omega)|$, open circles pip down, versus angular frequency ω. The dashed and solid curves represent η_κ and R_κ, respectively, for the solution. All responses are at 33°C.

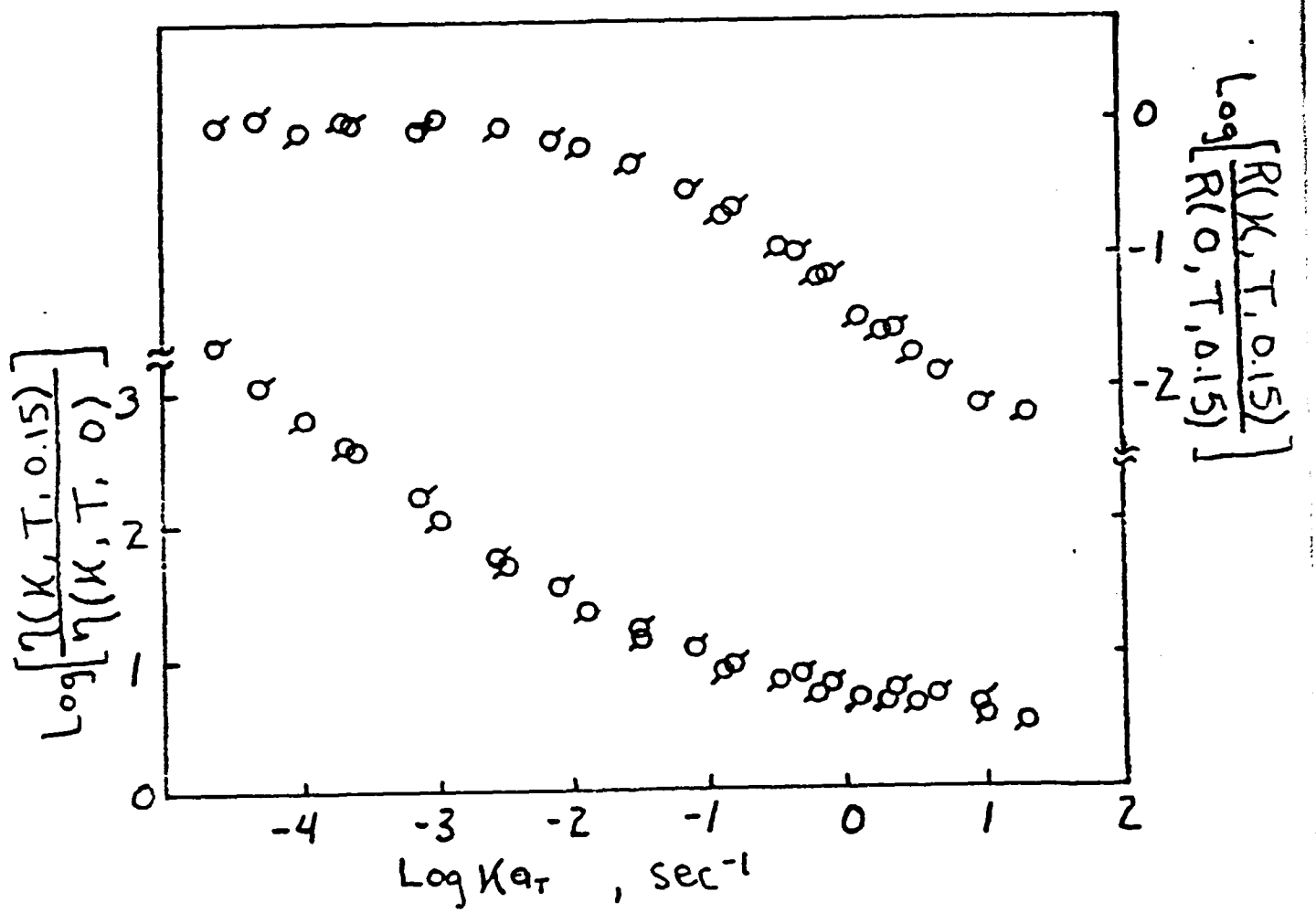

Figure 5:

The temperature superposition of η_κ and R_κ data for the 15% suspension in PS-DOP at 50°C (σ) and 30°C (ρ). The reference temperature is 50°C.

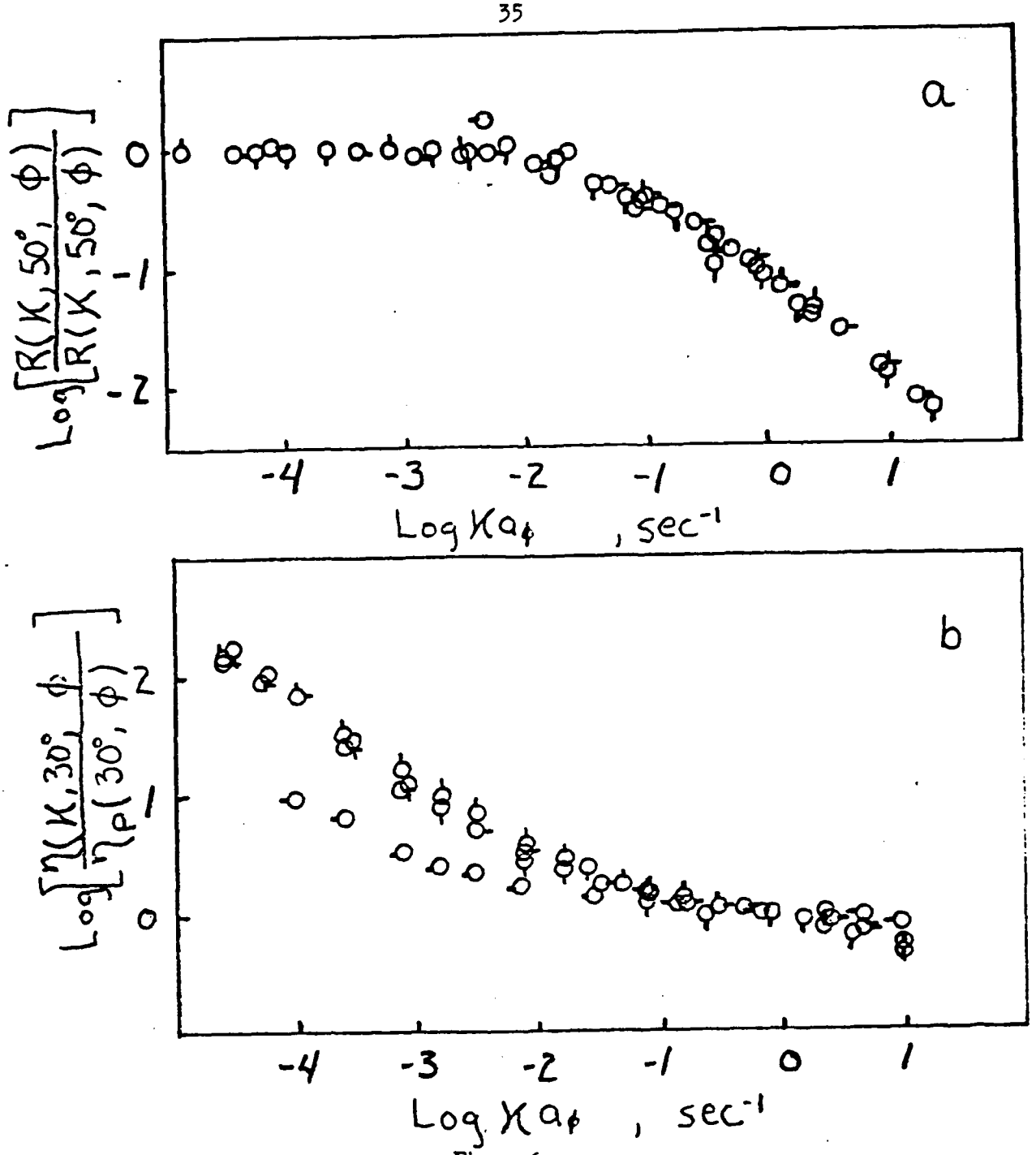

Figure 6:

Superposed plots of (a) R_κ and (b) η_κ for various concentrations of suspended particles as indicated by the same symbols as used in Figure 1. The reference concentration is 20%.

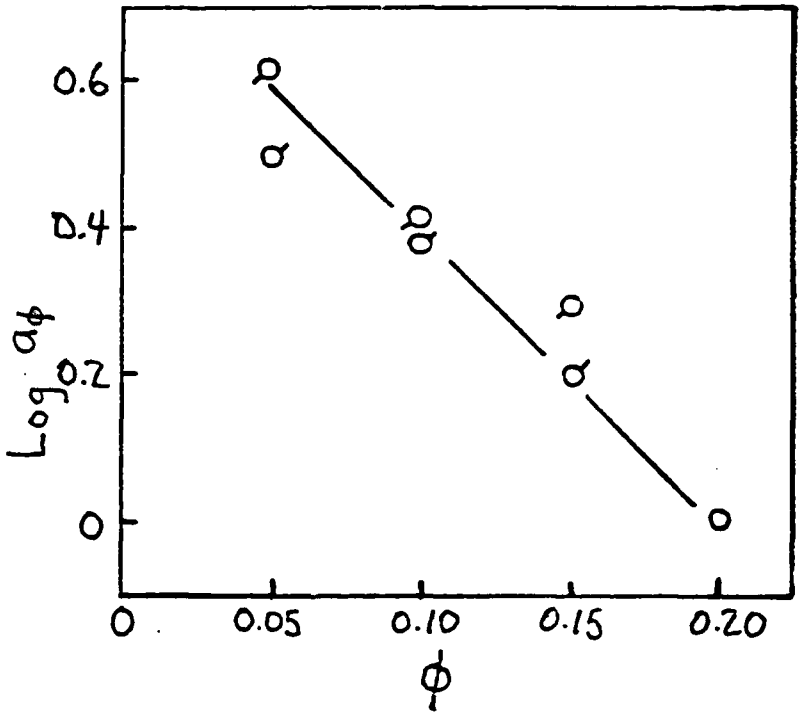

Figure 7:

Semilogarithmic plot of the concentration shift factor a_ϕ at 30°C and 50°C. The reference concentration is 20%. The temperature is indicated by the same symbols as used in Figure 5.

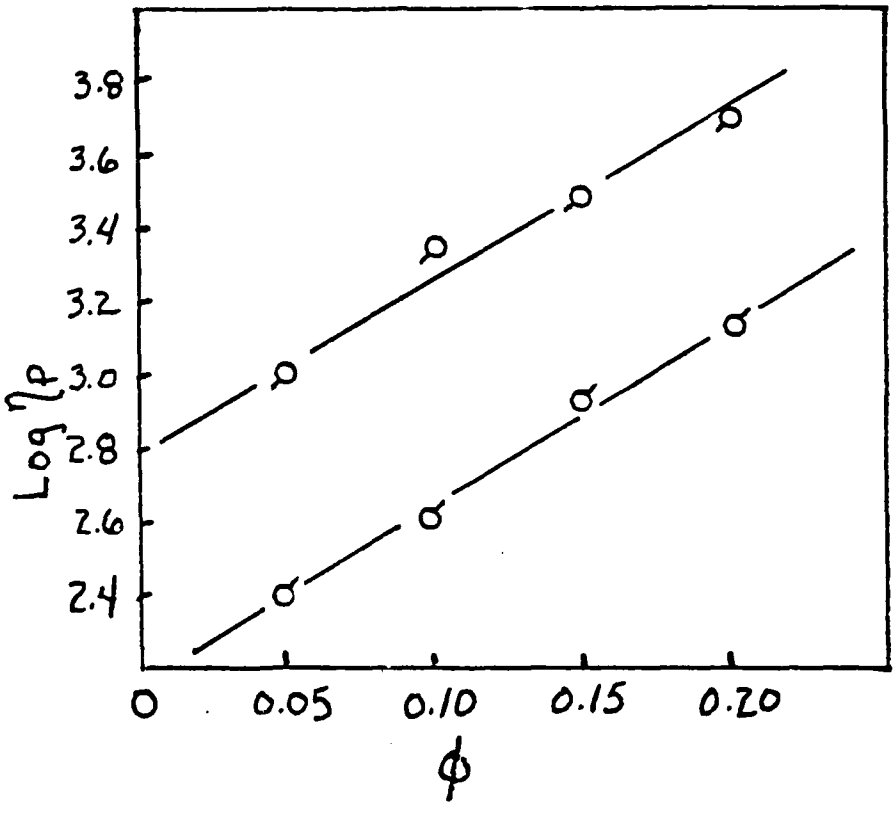

Figure 8:

Semilogarithmic plot of η_p as a function of the concentration of suspended particles at 30° and at 50°C as indicated by the same symbols as used in Figure 5.

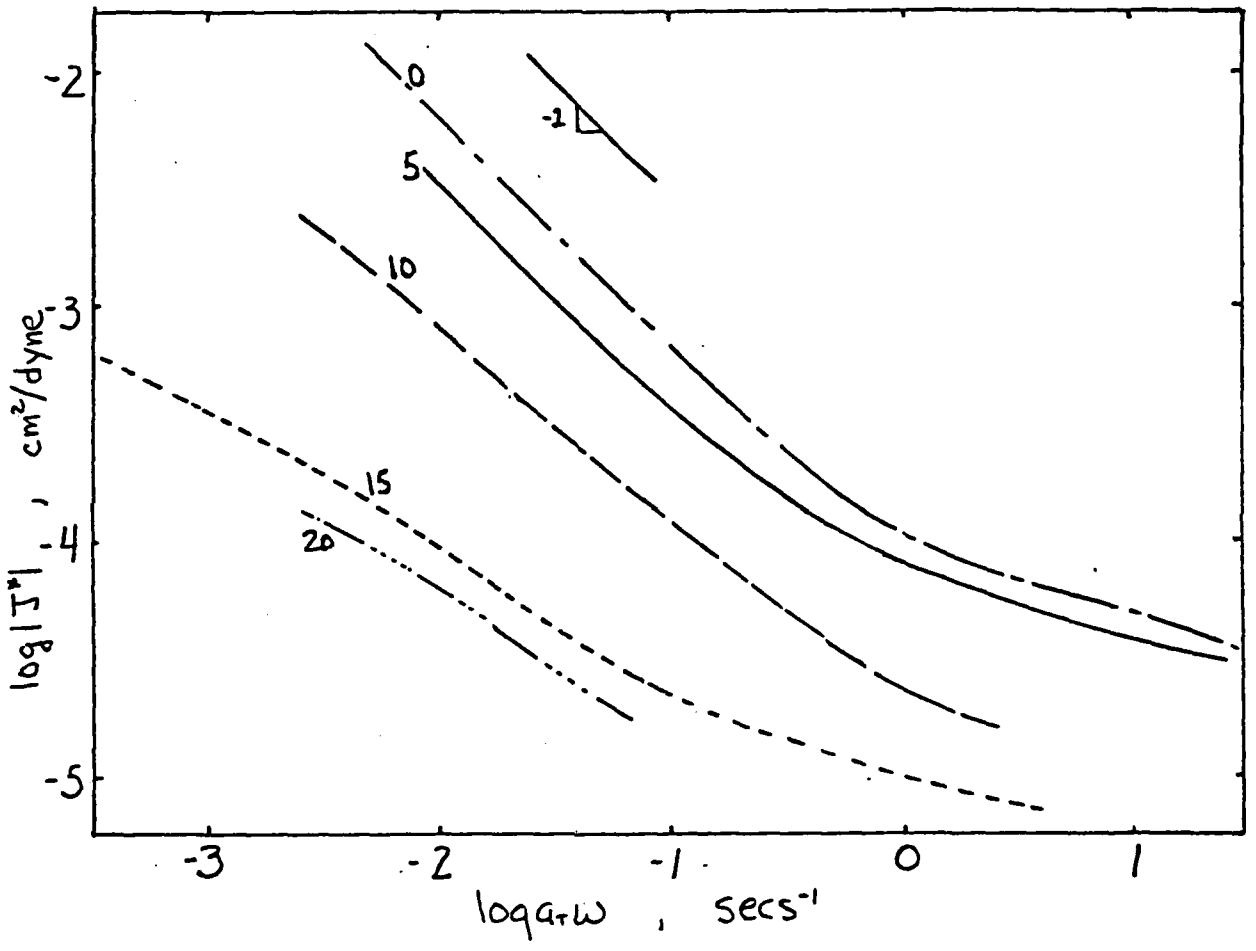

Figure 9:

Reduced bilogarithmic plot of the dynamic compliance $|J^*(\omega)|$ as a function of $a_T\omega$. The weight fraction of the suspended particles is indicated on each curve. The reference temperature T_0 is 0°C.

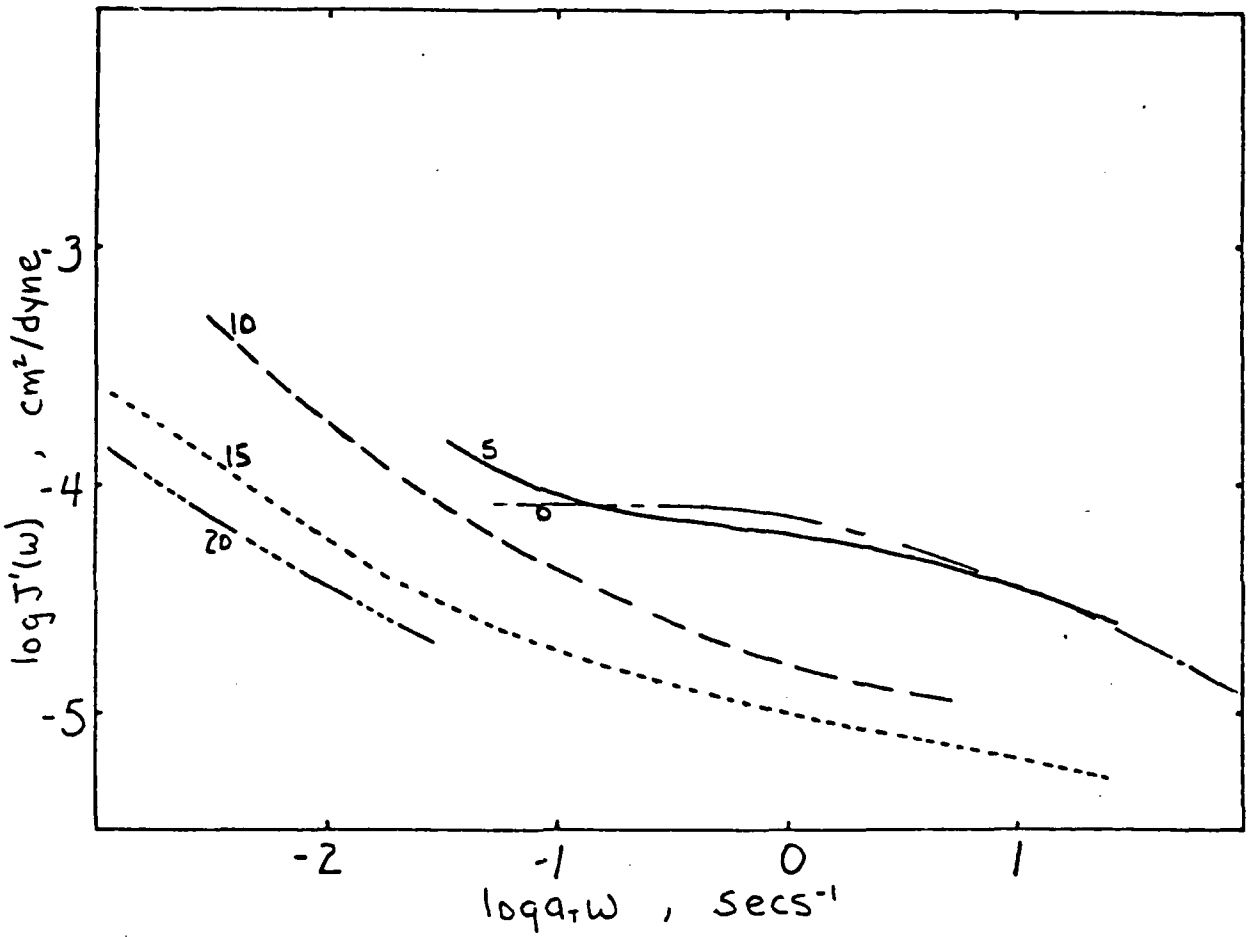

Figure 10:

Reduced bilogarithmic plot of storage compliance, $J'(\omega)$ as a function of $a_T\omega$. The weight fraction of the suspended particles is indicated on each curve. The reference temperature T_0 is 0°C.

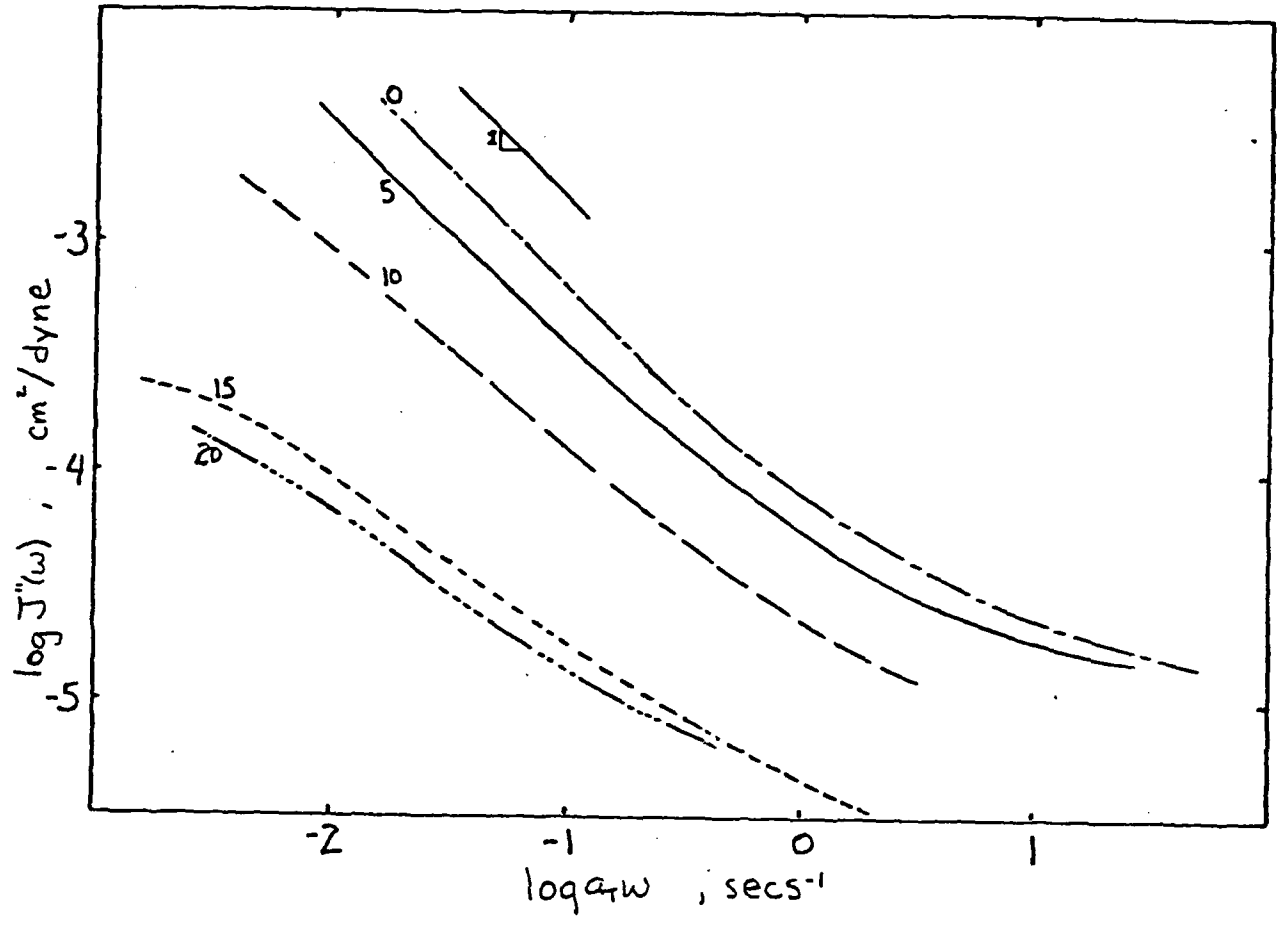

Figure 11:

Reduced bilogarithmic plot of the loss compliance, $J''(\omega)$ as a function of $a_T\omega$. The weight fraction of the suspended particles is indicated on each curve. The reference temperature T_0 is 0°C.

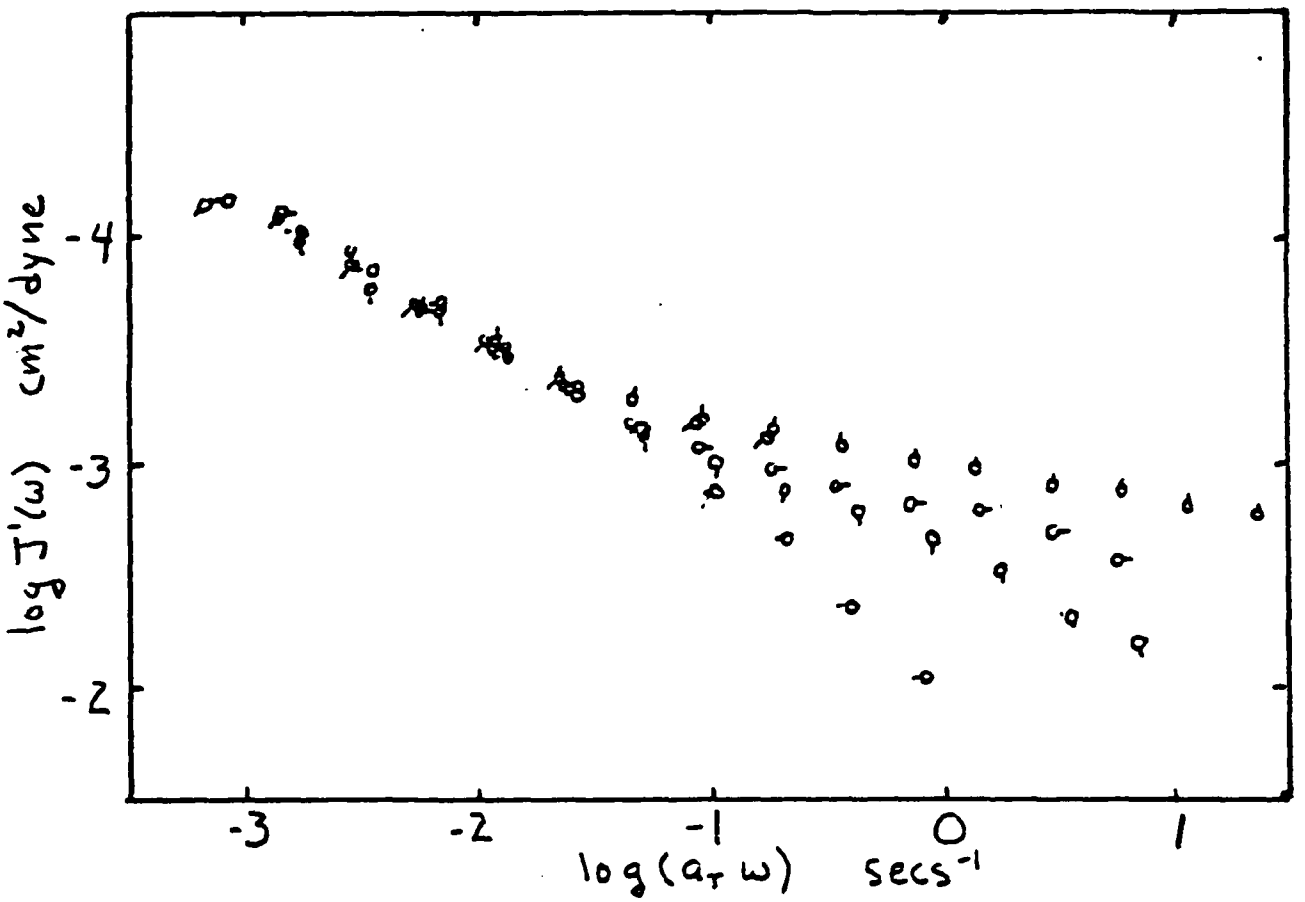

Figure 12:

Bilogarithmic plot of the storage compliance $J'(\omega)$ as a function of a_T for a 20% suspension of polystyrene beads in PS-TCP. Pips represent various temperatures, up 0.1°C, right 9.0°C, down 18.9°C, left 33.3°C. The reference temperature T_0 is 0°C.

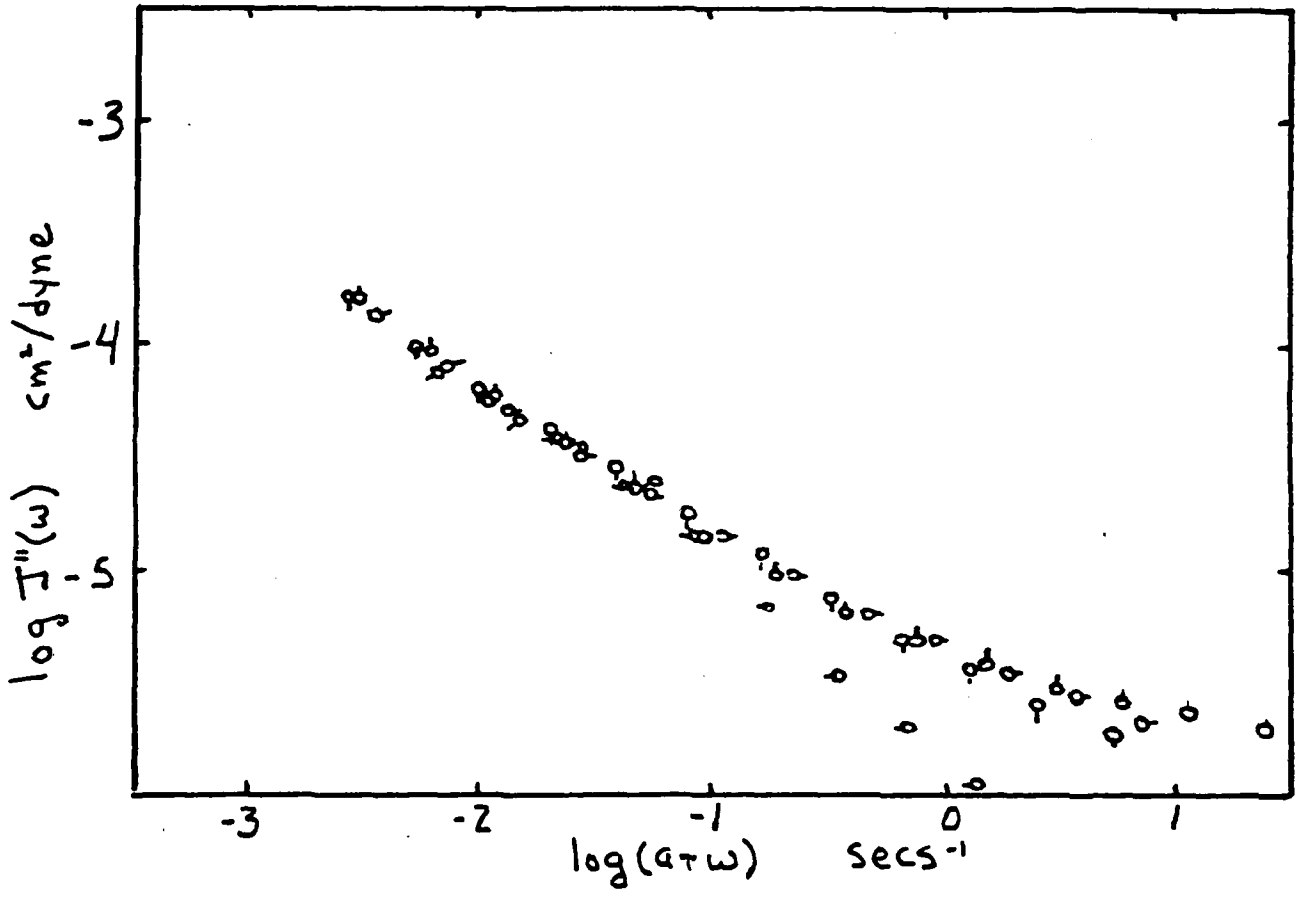

Figure 13:

Bilogarithmic plot of the loss compliance $J''(\omega)$ as a function of $a_T\omega$ for a 20% suspension of polystyrene beads in PS-TCP. Pips represent various temperatures, up 0.1°C, right 9.0°C, down 18.9°C, left 33.3°C. The reference T_0 is 0°C.

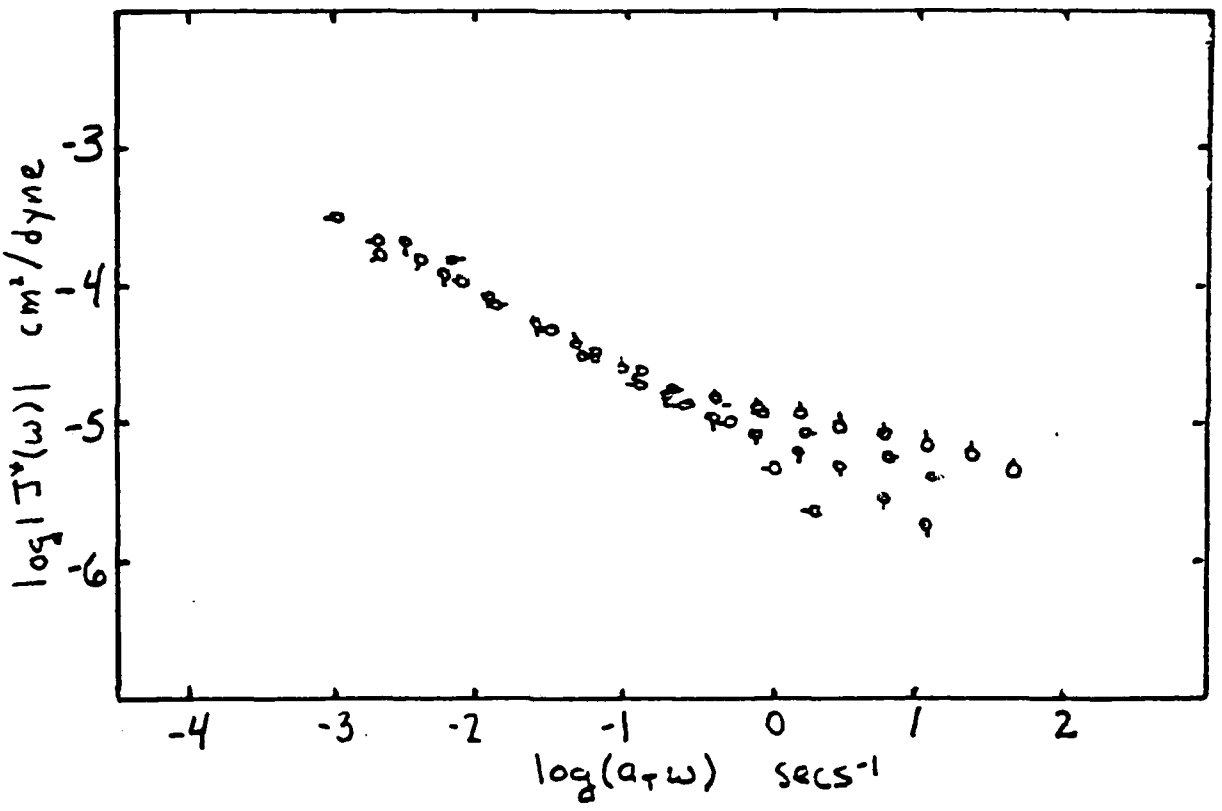

Figure 14:

Bilogarithmic plot of the dynamic compliance $|J^*(\omega)|$ as a function of $a_T\omega$ for a 20% suspension of polystyrene beads in PS-TCP. Pips represent various temperatures, up 0.1°C, right 9.0°C, down 18.9°C, left 33.3°C. The reference temperature T_0 is 0°C.

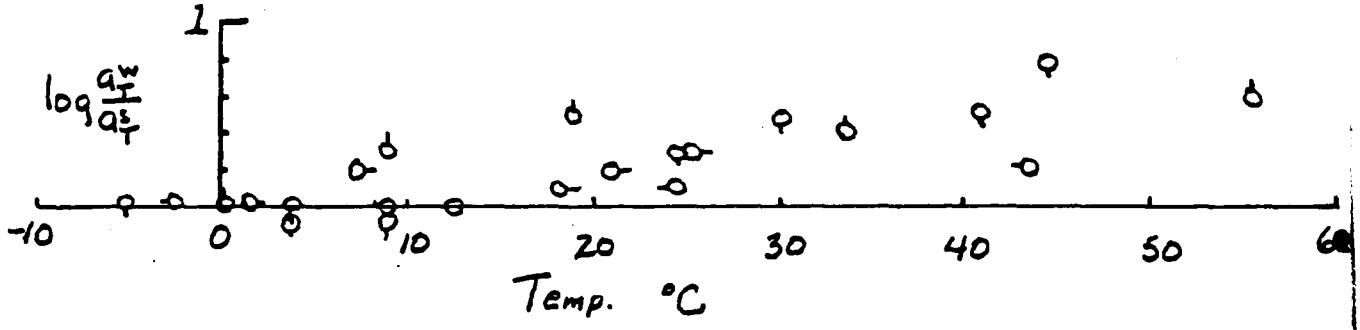

Figure 15:

Semilogarithmic plot of the shift factor for a given weight fraction a_T^w divided by the shift factor for the solvent a_T^s against temperature in °C. Pips represent various weight fraction right 0.05, down 0.10, left 0.25, and up 0.20. In each case the reference temperature T_0 is 0°C.

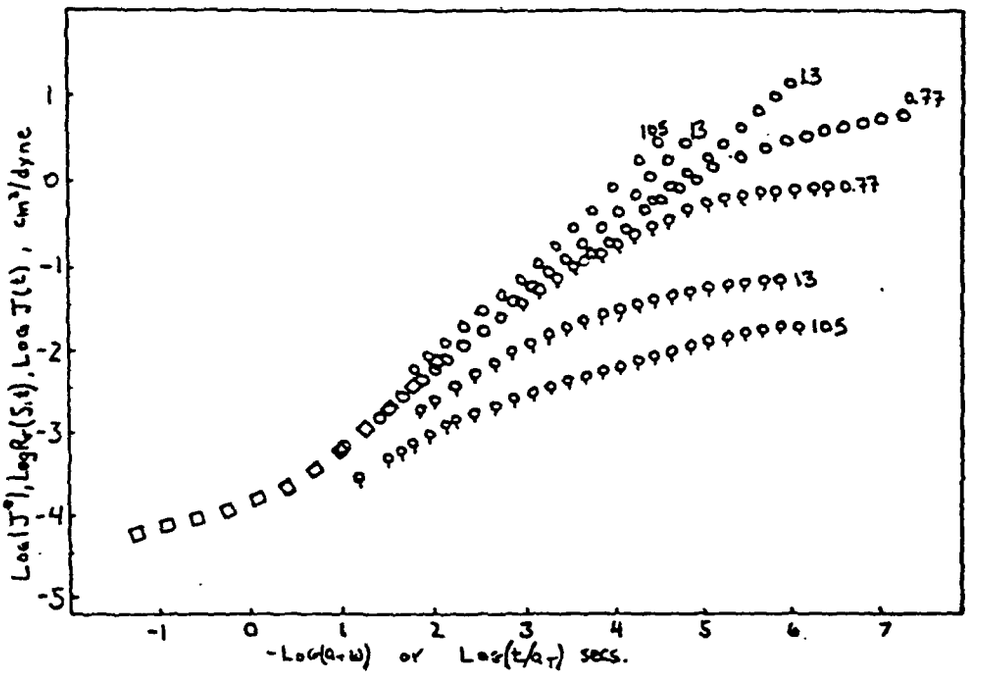

Figure 16:

Data for a 5% suspension of polystyrene beads in PS-TCP: Bilogarithmic plot of the creep compliance $J_\sigma(t)$ (no pips) and the recoverable compliance $R_\sigma(S,t)$ (pips down) versus ta_T^{-1} for the values of shear stress σ(dyn/cm^2) given on the figure — S is given by longest time for the corresponding creep experiment in each case. Bilogarithmic plot of the dynamic compliance $|J^*(\omega)|$ (squares) as a function of $(a_T\omega)^{-1}$ for comparison with $J_\sigma(t)$ at small strain (*i.e.*, short time).

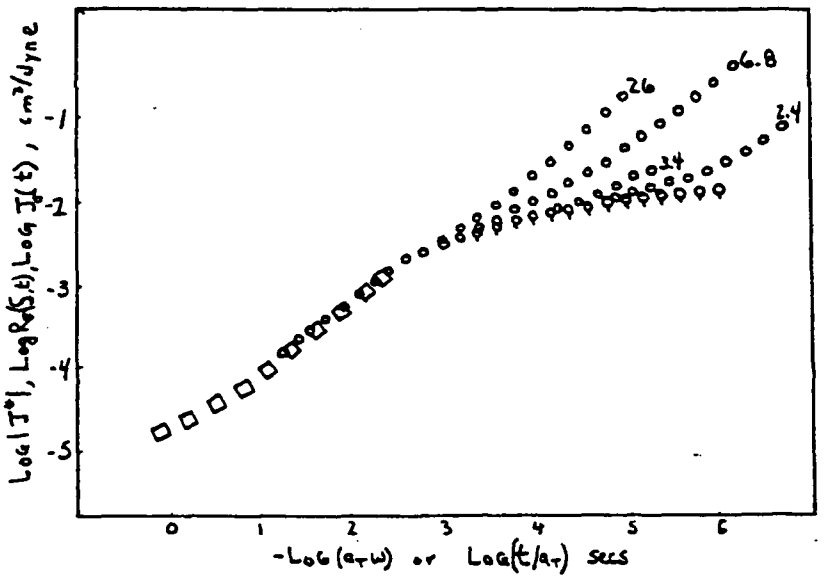

Figure 17:

Data for a 10% suspension of polystyrene beads in PS-TCP. Bilogarithmic plot of the creep compliance $J_\sigma(t)$ (no pips) and the recoverable compliance $R_\sigma(S,t)$ (pips down) versus ta_T^{-1} -- σ(dyn/cm^2) on the figure. S is large and the shear stress small so that the plot represents the limiting behavior $R_0(t)$ for this suspension. Bilogarithmic plot of the dynamic compliance $|J^*(\omega)|$ for comparison with $J_\sigma(t)$ at small strain (i.e., short time).

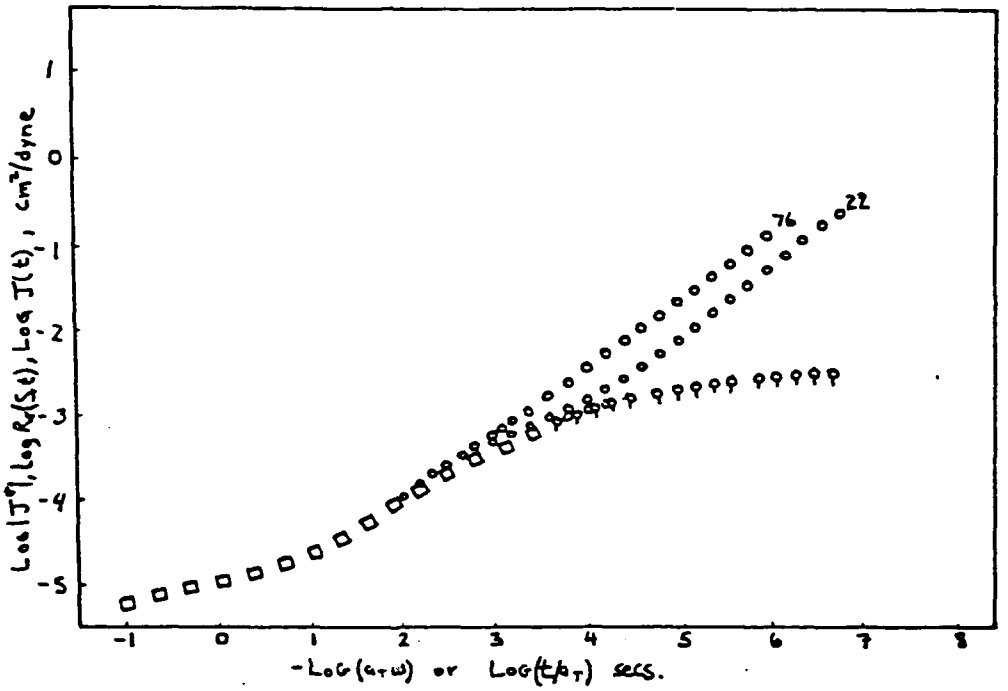

Figure 18:

Data for a 15% suspension of polystyrene beads in PS-TCP. Bilogarithmic plot of the creep compliance $J_\sigma(t)$ (no pips) and the recoverable compliance $R_\sigma(S,t)$ (pips down) versus ta_T^{-1} for the values of shear stress σ(dyn/cm^2) indicated on the figure. S is large and the shear stress small so that the plot represents the limiting behavior $R_0(t)$ for this suspension. Bilogarithmic plot of the dynamic compliance $|J^*(\omega)|$ (squares) as a function of $(a_T\omega)^{-1}$ for comparison with $J_\sigma(t)$ at small strain (e.g., short times).

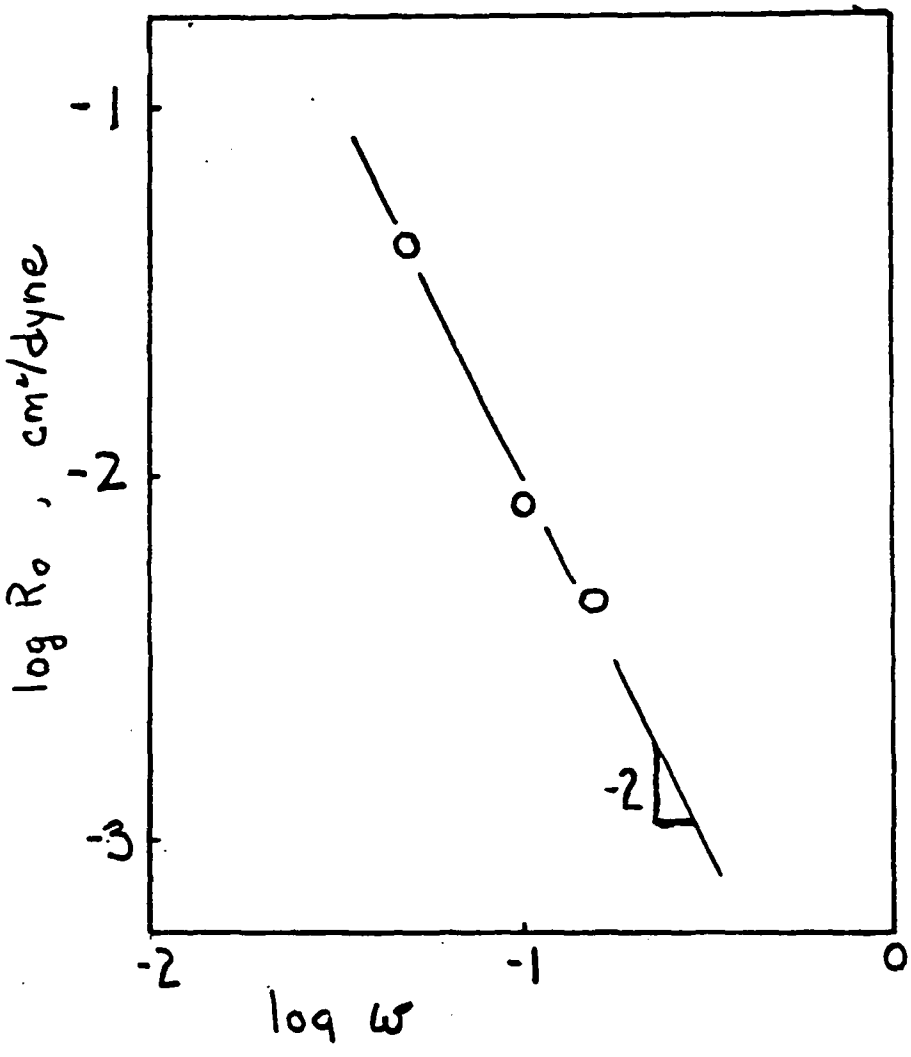

Figure 19:

Bilogarithmic plot of the limiting zero shear stress recoverable compliance R_0 versus w the weight fraction of suspended beads in the polystyrene fluid.

Figure 20:

Electron micrograph (50,000x)of a 15% suspension of polystyrene beads in PS-DOP.

III POLYMERIZATION KINETICS OF RIGID RODLIKE MOLECULES POLYCONDENSATION OF POLY BENZO 1,2-D 5,4-D BISOXAZOLE-2,6-DIYL -1,4-PHENYLENE PBO

David B. Cotts and Guy C. Berry

7 INTRODUCTION

The statistical analysis of polycondensation reactions is based on the understanding that reaction rates are independent of molecular weight.[1] The reactive end groups of flexible coils indeed diffuse, reorient, and react in solution at a rate independent of the polymer molecular weight. For rigid rods, however, diffusion of reactive end groups must be coordinated with that of the entire molecule. The transport properties[2] of rodlike molecules in general show a greatly enhanced dependence on molecular weight, in comparison with flexible macromolecules. In view of the extraordinary thermomechanical properties[3] that rodlike heteroaromatic polymers display, we have characterized the polymerization kinetics of poly[benzo(1,2-d:5,4-d')bisoxazole-2,6-diyl]-1,4-phenylene (PBO) to determine if shape anisotropy effects the polymerization process and its products. PBO is prepared by the step-growth polymerization of 4,6-diamino-1,3-benzenediol (DBD) and terephthalic acid (TA):

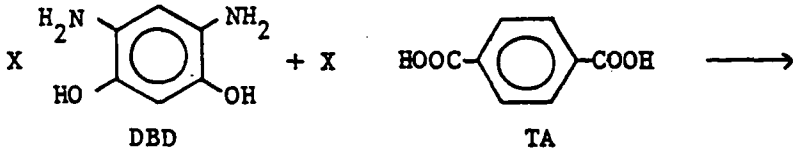

DBD TA

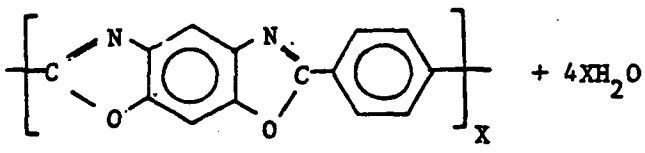

PBO

The reaction is carried out in polyphosphoric acid (PPA), which serves to remove the water formed in the polymerization step.

8 EXPERIMENTAL

The monomer 4,6-diamino-1,3-benzenediol dihydrochloride was synthesized using conditions reported in reference 9. Polymerizations were carried out in freshly prepared polyphosphoric acid, (85% P_2O_5) following the general procedure outlined in reference 9, but several important features were changed to facilitate quantitative kinetic analysis. To avoid complications due to the ordering of polymer molecules in liquid crystalline domains, polymerizations were performed at concentrations of 0.5 to 2.0 weight percent polymer. These concentrations were low enough that none of the reaction mixtures were birefringent when observed through crossed polars at room temperature, indicating that ordered domains were not present. A further advantage of dilute solution polymerization is that the solution viscosity remains low enough for adequate stirring and for samples to be withdrawn throughout the reaction with a syringe and Teflon® needle while preserving an inert atmosphere in the polymerization vessel. At this dilute concentration, the dihydrochloride monomer could be dehydrochlorinated within a few hours and the solution brought to the polymerization temperature by immersion in an oil bath controlled to ±0.1°C. The reaction was begun with the addition of a stoichiometric quantity of finely divided terephthalic acid, followed by vigorous stirring.

Small reaction samples (∿1 g) were precipitated in a 100-fold excess of water. The supernatant was analyzed for monomer content by UV absorption spectroscopy. Control experiments on mixtures of PBO and the monomers showed that the monomer remained in the supernatant fluid, and could be easily detected. Larger samples (∿20 g) were precipitated into

a large excess of water, collected, and washed with water in a soxhlet extractor for 12 h to remove residual polyphosphoric acid. The polymer was then freeze-dried from water and dried under high vacuum before further analysis.

Intrinsic viscosity measurements were performed in Ubbelohde viscometers at 30 ±0.01°C. Vacuum distilled methanesulfonic acid (MSA) and chlorosulfonic acid (CSA) were each used as the solvent. Capillaries were chosen to provide solvent flow times in excess of 150 s and no kinetic energy correction was needed. Measurements with several capillaries revealed no shear rate dependence.

Infrared absorption spectra were recorded on finely ground KBr pellets with a Perkin-Elmer 580 Spectrometer. The ratio r of absorbance for the repeat group (benzoxazole, absorbing at 1630 cm^{-1}) and end group (carbonyl, absorbing at 1700 cm^{-1}) was used to compute the number average molecular weight. Mixtures of terephthalic acid and 2,2'-diphenylbenzobisoxazole were used to obtain r over a range of benzoxazole to carbonyl ratios to evaluate the method and determine r_0 corresponding to the moiety

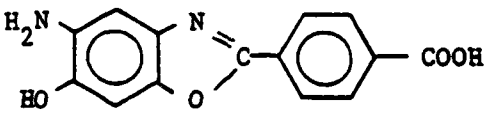

The results gave $r_0 = 4.35 \times 10^{-2}$. The number average degree of polymerization x_n was obtained from the expression

$$x_n = r/2r_0$$

where the factor of 1/2 is necessary because there are two benzoxazole

rings per repeat unit and an average of one carbonyl end group per chain.

UV-VIS absorption spectra of the supernatant from reaction precipitation and of polymer solutions in MSA and CSA were recorded with a Cary 14 spectrometer. Size exclusion chromatography (SEC) characterization was performed with an instrument designed for use with solutions of polymers in strong acid solvents.[10] The effluent concentration was monitored by absorption at 425 nm using a Spec-21 spectrometer. The data were interpreted using a universal calibration in terms of intrinsic viscosity-molecular weight product $[\eta]M$ as a function of elution volume, obtained with narrow molecular weight polystyrene standards in various solvents.

Molecular theories for the intrinsic viscosity of rigid rodlike molecules indicate that the molecular weight dependence of the intrinsic viscosity may be expressed as[11]

$$[\eta] = 5.81 \times 10^{20} d_H^{0.2} M_L^{-1} L^{1.8} \quad (1)$$

or

$$M[\eta] = 2.70 \times 10^{-7} M^{2.8} \quad (2)$$

obtained by substituting the appropriate values of the hydrodynamic diameter d_H and the mass per unit length M_L equal to the molecular weight M divided by the chain length L. Using Eqn (2), average molecular weights, the molecular weight distrubition, and the intrinsic viscosity can be calculated from the chromatogram of $M[\eta]$ versus (relative) concentration.

In principle, the analysis would be enhanced by collection and concentration of the fractions from the SEC to permit measurement of molecular weight and intrinsic viscosity for each. Unfortunately, precipitation of this and other aromatic heterocyclic polymers leads to irreversible

morphological changes preventing complete redissolution,[11,12] making such a tactic unreliable.

9 RESULTS

The UV-VIS absorption spectra of the supernatant fluid recovered on precipitation of an aliquot from the polymerization reaction did not contain absorption bands due to either monomer. Control experiments indicate that both monomers are quantitatively extracted from the water insoluble polymer on precipitation. The minimum detectable concentration (0.01 Absorbance Units) of DBD in aqueous solution is $\sim 10^{-6}$ g/ml which with our reaction workup (100 fold dilution) corresponds to a concentration in the reaction medium of 10^{-4} g/ml. The analytical procedures therefore are sensitive to monomer concentrations several orders of magnitude below that which would be expected for the conversions encountered in this study. The absorption spectra, which give zero absorbance for wavelengths greater than 240 nm, indicate the absence of soluble side products or incompletely cyclized, e.g., hydroxyamide, condensation products.

In typical polycondensation reactions, monomer molecules are the most prevalent species by number throughout the reaction. The enhanced consumption of monomer resulting from intrinsic reactivity differences has been observed in other systems,[4,5,6] but only in one system[4] has the complete consumption of monomer been observed at such a low extent of reaction.

The intrinsic viscosities in MSA of the samples produced in this study are shown in Figure 1 as a function of reaction time and temperature. Our experience with measurements of the intrinsic viscosity of PBO and other aromatic heterocyclic polymers has consistently shown that the data are very difficult to interpret. Both reversible and irreversible

aggregation are thought to occur as a result of variations in concentration and solution history (e.g., workup of the polymerization reaction, reprecipitation, trace quantities of moisture). These data may therefore be used as an indication of the extent of reaction, but they do not at this time warrant a quantitative analysis.

Typical SEC results obtained for a series of polymerization aliquots are shown in Figure 2. Quantitative SEC analysis[13] requires that all polymers eluted at a specific elution volume share a constant $[\eta]M$ product. The molecular weight distribution may then be calculated with the use of a relation between $[\eta]$ and M, such as Eqn. 1. Comparisons of M_n obtained by end group analysis and SEC given in Figure 3 show general agreement between the two methods for M_n less than 4,000. For larger M_n, data (not shown) consistently gave larger M_n by the IR method, probably owing to the difficulty of properly determining areas of the absorption bands when the carbonyl absorption is very weak. Nonetheless, the limited comparison is of value because the IR analysis is immune to the effects of aggregation that complicate the dilute solution characterization. Molecular weights obtained by SEC analysis are plotted in Figures 3 and 4 as a function of reaction time, temperature, and concentration. Eqn. (2) is of the form $[\eta]M=KM^b$. Use of different values of K and b than those given by Eqn. (2)

to calculate M_n and M_w/M_n will vary the absolute numbers, but not the overall qualitative character of the results; calculation of M_w/M_n does not depend on K and is insensitive to b for reasonable values of b.

The presence of side reactions that consume reactive end groups could bring about the decreasing rate of growth in the molecular weight observed in Figures 3 and 4. The amine monomer is highly sensitive to oxidation, especially at these high temperatures. However, degradation products, which are readily detected because of their intense red color, were not present in any of these polymerization reactions. Moreover, amine monomer appears to be stable for periods of several days under reaction conditions. For example, analysis by UV-US absorption spectroscopy of a 1% solution of DBD in PPA stirred at 150°C for 48 hours revealed neither the formation of degradation products nor the loss of more than 0.10% of the monomer.

Second-order reaction statistics, which should apply to condensation in acidic solvents, require that the rate of increase in the number average molecular weight, dM_n/dt, be constant and proportional to the rate of polymerization:

$$x_n = [M]_o kt + \text{Const.} \qquad (3)$$

where $[M]_o$ is the initial monomer concentration and X_n is the number average degree of polymerization. The data in Figures 3 and 4 are clearly not consistent with a single-rate process. Early stages of the reaction, however, appear to be linear. The apparent rate constants $[M]_o k$ plotted versus inverse temperature in Figure 5 yield an activation energy of 7.16 Kcal/mol . This value is somewhat higher than the flow activation energy for PPA of 3.7 Kcal/mol. Values of $[M]_o k$ determined at 185°C for initial monomer concentrations of 0.5, 1.0 and 2.0 weight percent (Figure 4) gave $k = 5.3 \times 10^4$ ℓ $mol^{-1}h^{-1}$ for each concentration, consistent with the assumed second-order kinetics.

Further evidence for a polymerization rate dependent on the molecular weight may be found in an analysis of the molecular weight distribution and polydispersity ratios. Figure 6 shows that throughout the polymerization, the polydispersity ratio M_w/M_n is consistently lower than that calculated on the basis of the most probable reaction statistics, and only approaches the limiting value of 2.0 at extremely high conversions. Figure 7 shows comparison of the actual experimental molecular weight distribution for a sample with a degree of polymerization of 30 with one calculated for most probably reaction statistics at an equal number-average degree of polymerization. An important feature is the depletion of components with very low and high chain lengths. It should be mentioned that SEC measurements over a wide range of conversion indicate that the column exclusion limits have not been approached, as shown by Figure 2.

10 DISCUSSION

The observed effects on the rate of conversion and the molecular weight distribution can be understood in terms of a polymerization rate constant k_p that depends markedly on the chain lengths of the reactants. The rate of disappearance of components with chain length x_i is given by the relation

$$-\frac{d[P_i]}{dt} = [P_i]\ \Sigma k_p(i,j)[P_j] - (1/2)\ \Sigma k_p(i-j,\ j)\ [P_{i-j}][P_j] \qquad (4)$$

where the sums extend over all components identified by degree of polymerization x_i, and the total molal concentration $[P] = \Sigma[P_i]$. A coupled set of such equations is required to describe the polymerization

kinetics. With flexible chain polymers, k_p is independent of chain length (except for x_i less than about 3-4 in some cases), and k_p may be factored out of the sum. This condition is brought about by the effects of segmental motion, which renders the collision frequency of chain ends independent of the chain length, and by compensating effects on diffusion of the reactive ends into and out of the reactive transition state. With the latter, decreased molecular mobility increases the time required to form a transition state, but lengthens the time such a state persists.[1]

A strongly chain length dependent diffusion constant will alter this situation. If the time τ_D required to form the transition state necessary for condensation is longer than the lifetime τ_E of that state (e.g., the time required for either reaction or separation of the end groups), the rate limiting step is the formation of a transition state. The rate limiting step is therefore not the rate at which molecules which have obtained the necessary colinear alignment successfully condense, but the rate at which that colinear alignment is formed. In the extreme, all molecules which achieve colinearity and proximity condense, and the polymerization rate is controlled by the rate at which that transition state is formed.

With PBO, the cyclization can only be completed if the rodlike chains are aligned colinearly; intermediate partially cyclized products have not been found and are presumably not stable in PPA. Because of this required colinearity, τ_D for PBO might be limited by the rotational time constant τ_R, which is proportional to x^3 for dilute solutions, and is even more markedly dependent on x for moderately concentrated solutions.[14] Simple translation along the chain axis, with

time constant τ_T about proportional to x, will suffice to destroy the transition state if reaction does not occur. An analogous situation is found in some bulk free radical polymerizations at high conversions, for which τ_D for formation of a transition state of a pair of macroradicals becomes very long compared to the lifetime of the transition states, causing the termination rate constant to decrease in comparison with the propagation rate constant. The latter is relatively unaffected by conversion, as the time to form a transition state of monomer and macoradical is controlled by monomer diffusion.

During the phase of the reaction studied for which the number average degree of polymerization $x_n > 10$, it is found that

(1) The quantity dx_n/dt decreases rapidly with increasing conversion for x_n greater than about 20,

(2) The molecular weight distribution is sharper than expected for an equilibrium step-growth polymerization,

(3) The distribution is depleted in low molecular weight components, and

(4) The apparent activation energy of the polymerization (7.16 kcal/mol) is comparable to that for viscous flow of the polymerization solvent.

These observations are consistent with substantial dependence of $k_p(i,j)$ on the chain lengths x_i and x_j of the reactants. This seems reasonable in view of the low mobility of the reactant species, the extreme dependence of τ_R on x that is expected, and the disparity between $\tau_D \sim \tau_R$ and $\tau_E > \tau_T$.

Two additional features of the polymerization are noteworthy; no monomer was found in the polymerization aliquots (all taken after x_n had advanced to about 5), and the data for x_n versus t do not extrapolate to dimer, as expected, unless the initial rate is allowed to be much greater than that observed for x_n greater than 10. The latter may reflect the postulated dependence of $k_p(i,j)$ on chain length, since $k_p(i.j)$ might be expected to decrease most rapidly with increasing chain length for small chain lengths. The rapid loss of monomer observed may involve intrinsic difference in the reactivity of the end group on the monomer as compared with those of oligomers. Such differences have been observed in the polymerization of flexible chain polymers, but usually have negligible influence beyond a chain length of 3-4 repeating units. The effects of protonation of the monomer and oligomers in PPA on the electronic state may play a role in any intrinsic difference in reactivity, as was suggested by similar behavior for polymerization of a heterocyclic flexible chain polymer in PPA.[4] In that case, the rapid loss of monomer is not directly related to the subsequent effects on dM_n/dt and M_w/M_n as functions of polymerization time.

A definitive analysis of the data given here would require a reaction rate theory to relate $k_p(i,j)$ to τ_E and τ_D, and is beyond the scope of this study. It may be noted, however that τ_D does not have to be excessively long on an absolute scale for the effects enumerated above to be observed, but merely long compared with τ_E, and strongly dependent on x. Although these conditions are not met with flexible chain polymers, the severely decreased mobility of the rodlike chains appears to foster conditions in which condensation proceeds through a mechanism which can

not be modeled by equilibrium step-growth polymerization statistics. Numerical calculations by Peebles and coworkers[7] for polymerizations with $k_p(i,j) \propto x_i^{-r} + x_j^{-r}$ simulate some of the features observed here (e.g., a decreasing rate of polymerization with increased conversion, and a narrowed molecular weight distribution), but the model appears too arbitrary to apply meaningfully to the limited results reported here.

The tendency noted in Figure 6 for M_w/M_n to approach the limit 2 expected of an equilibrium step-growth polymerization implies that the terms $k_p(k,j)[P_i][P_j]$ in Eqn. (4) tend to become independent of the chain length of the reactants at high conversion. This is to be expected in that as chain lengths increase their rotational diffusion constants asympotically approach zero. The difference in the rate at which molecules reorient decreases, relative to the differences between smaller oligomers, and the conditions necessary for equal reactivity are approached.

11 REFERENCES

1. P.J. Flory, "Principles of Polymer Chemistry", Cornell University Press, Ithaca, NY, 1953, p. 75.

2. C. Tanford, "Physical Chemistry Macromolecules", Chapter 6, p. 317, J. Wiley and Sons, NY, 1961.

3. S.R. Allen, A.G. Filippov, F.J. Farris, E.L. Thomas, C.P. Wong, G.C. Berry, and E.C. Chenevey, Macromolecules, in press.

4. V. Ammons and G.C. Berry, J. Poly. Sci., 10:449 (1972).

5. R. Challa, Die Makromolecular Chemie, 38:105 (1960).

6. K. Gupta, et al., Polymer, 18:851 (1977).

7. L.H. Peebles, personal communication.

8. V. Nanda and S. Jain, J. Chem. Phys., 49:1318 (1968).

9. J.F. Wolfe and F.E. Arnold, Macromolecules, in press.

10. G.C. Berry and S.P. Yen, "Symposium on Polymerization and Polycondensation", (R.F. Gould, ed.), American Chemical Society, 1970, p. 734.

11. P.M. Cotts, Ph.D. Thesis, Carnegie-Mellon University, 1979.

12. G.C. Berry, J. Poly. Sci., Symposium, 65:78 (1979).

13. A.C. Ouano, "Polymer Molecular Weights", (P. Slade, ed.), Part 2, M. Dekker, NY, 1975, p. 287.

14. M. Doi and S.F. Edwards, J. Chem. Soc. Farad Trans II, 74:560, 918 (1978).

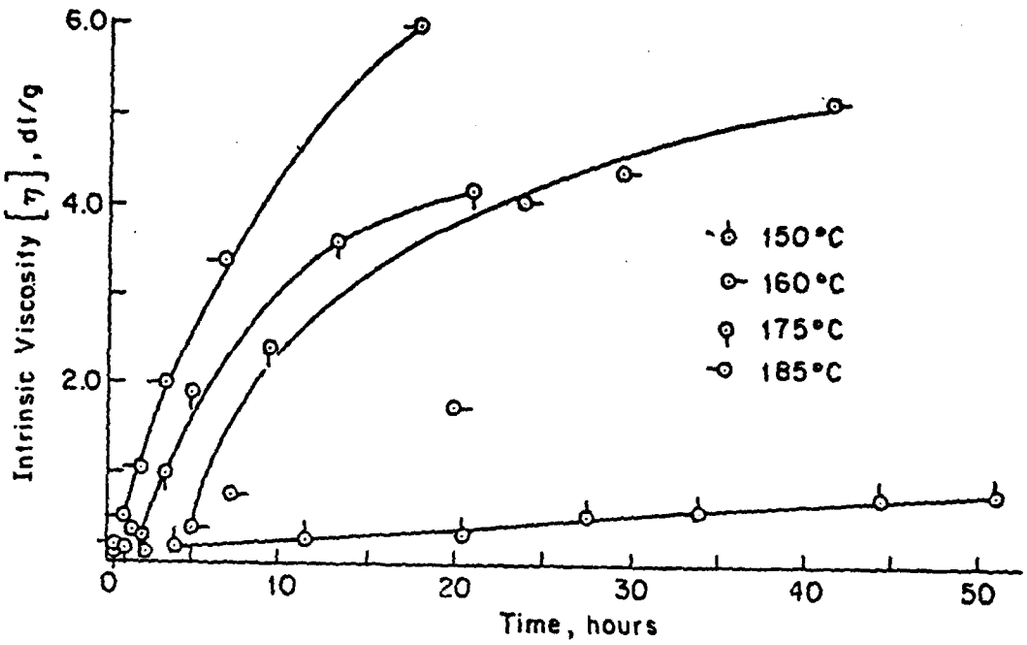

Figure 1. Intrinsic viscosity (MSA at 30°C) versus polymerization time for reactions at several temperatures as indicated; initial monomer concentration 1% by weight.

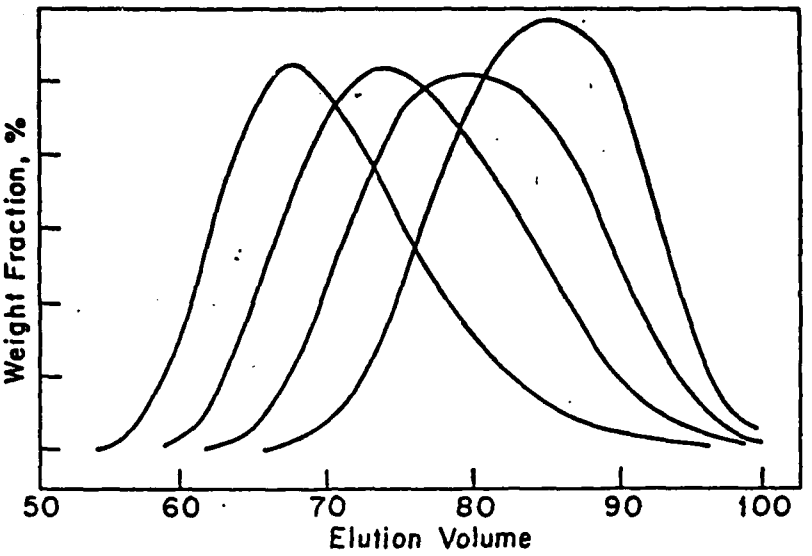

Figure 2. Size exclusion chromatograms for alequots obtained at reaction times of 1, 2, 3 , and 7 hr from right to left, respectively; polymerization at 185°C with initial monomer concentration 1% by weight.

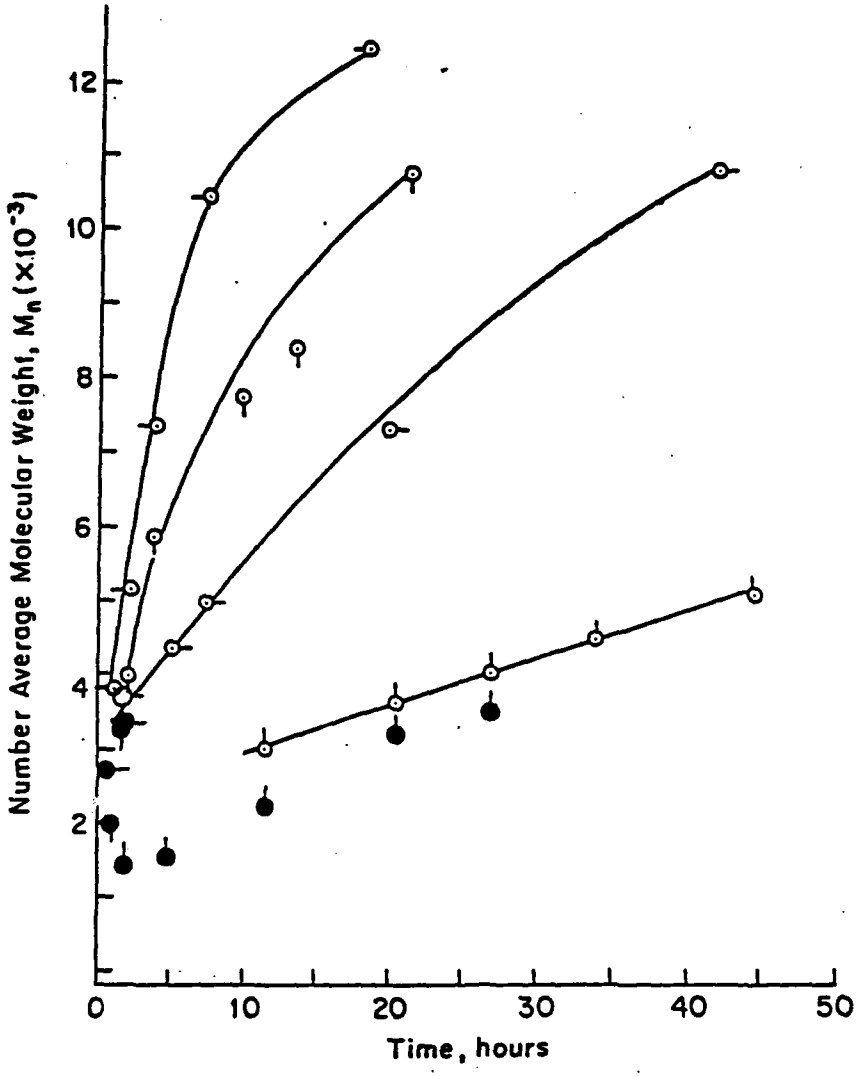

Figure 3. Number average molecular weight versus polymerization time for reactions at several temperatures as designated in Figure 1. M_n from SEC, ○, and IR analysis, ●.

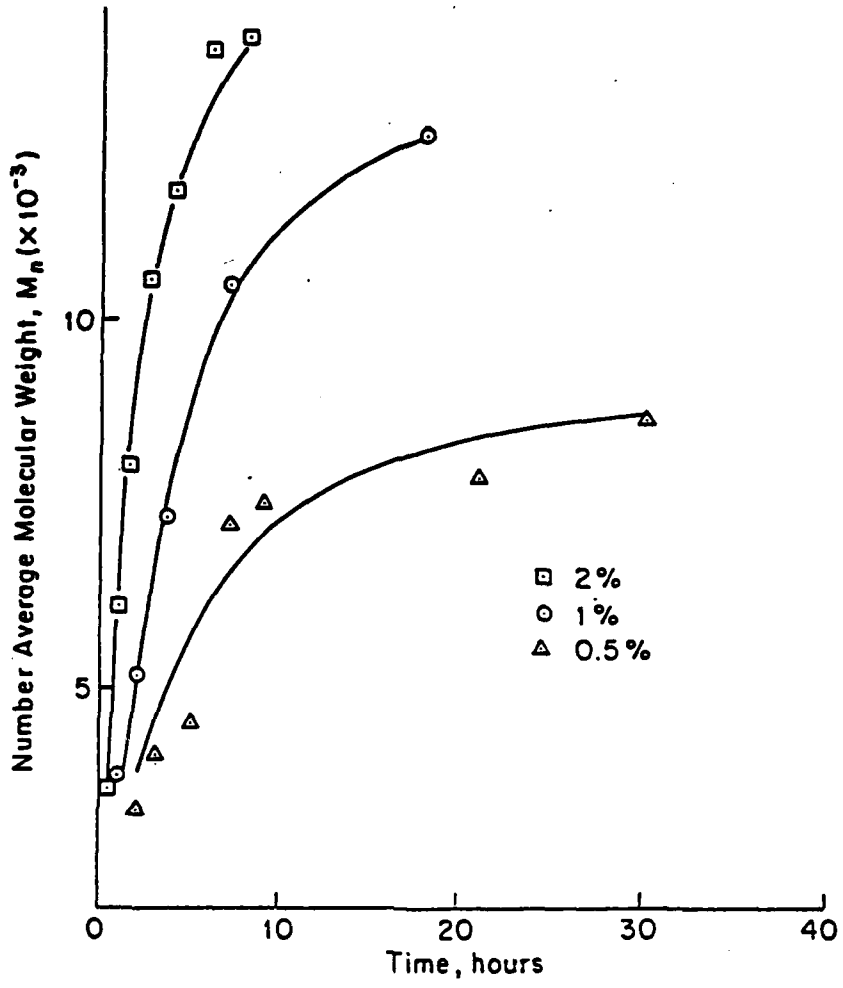

Figure 4. Number average molecular weight (from SEC analysis) versus polymerization time for reactions with initial monomer concentration as indicated; polymerization temperature.

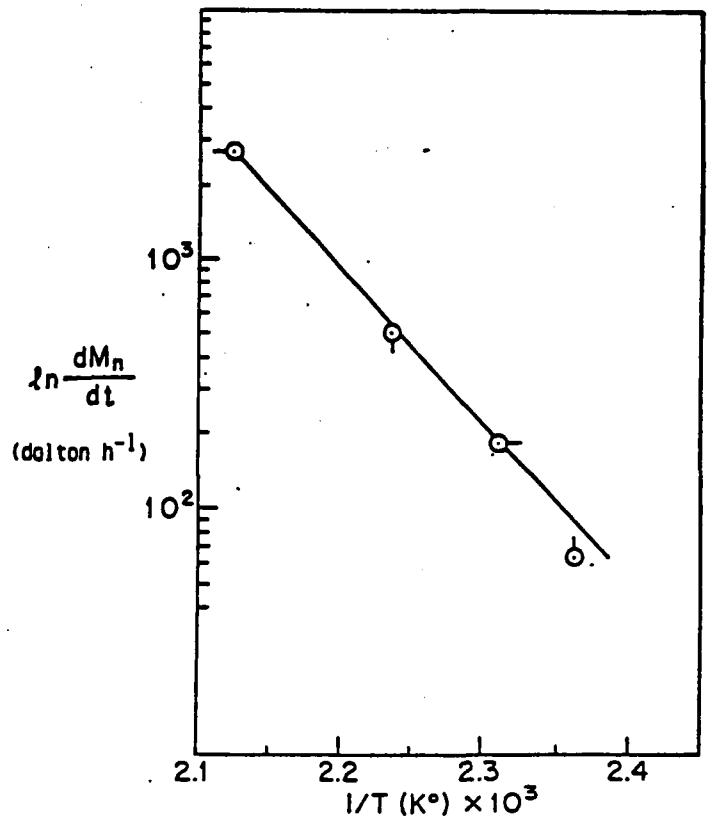

Figure 5. Plot of $\ln(\partial M_n/\partial t)$ versus reciprocal temperature for data from the initial part of the reaction; initial monomer concentration 1% by weight.

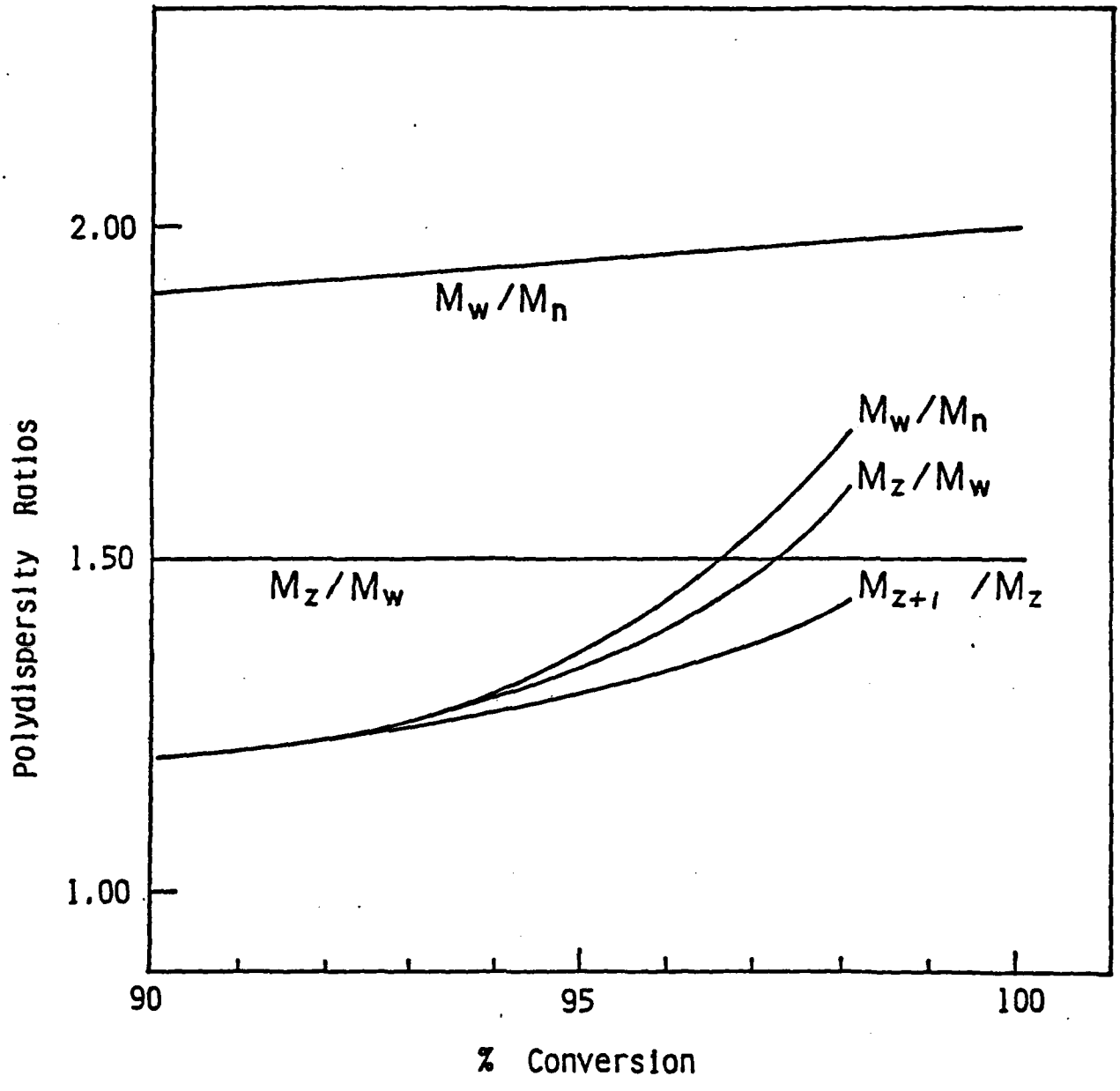

Figure 6. Polydispersity ratios as a function conversion for most probable reaction statistics (straight lines) and experimental data.

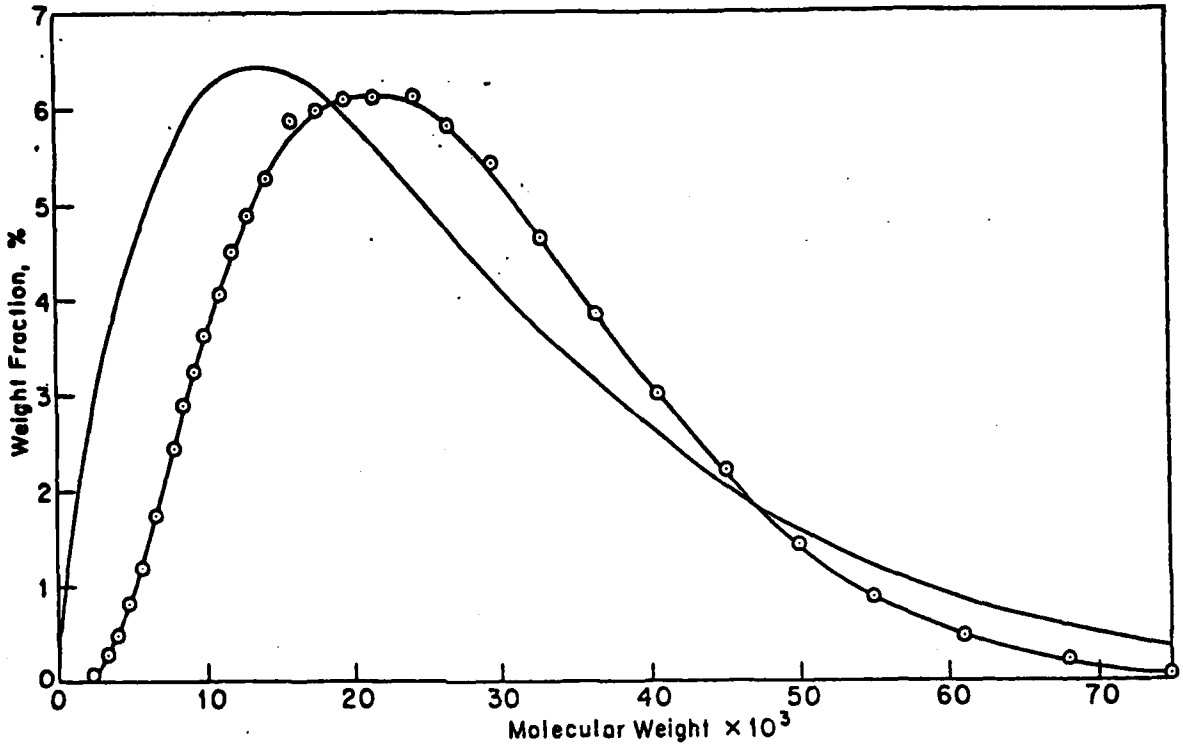

Figure 7. Experimental (-⊙-) and most probable (——) molecular weight distributions at equal number average molecular weights.

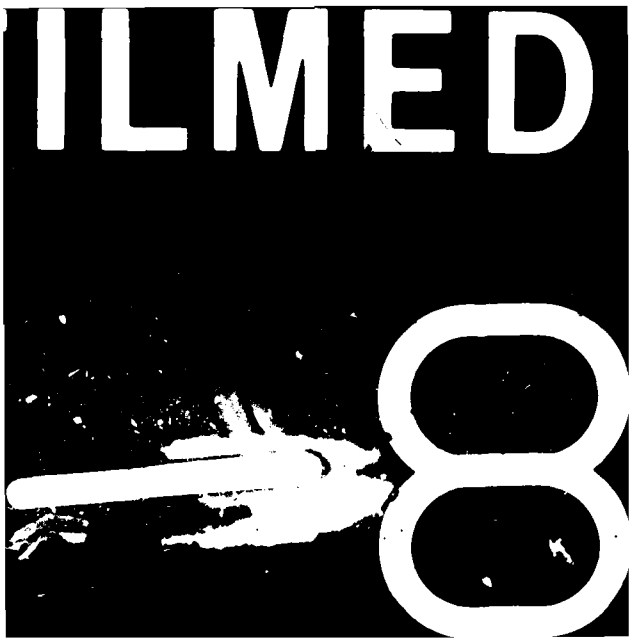
ILMED
8